Coordination Chemistry Reviews 471 (2022) 214738

Contents lists available at ScienceDirect

Coordination Chemistry Reviews

journal homepage: www.elsevier.com/locate/ccr

Review

Layered double hydroxides-based materials as novel catalysts for gaseous VOCs abatement: Recent advances and mechanisms

Qi Yu [a,b], Caiting Li [a,b,*], Dengsheng Ma [a,b], Jungang Zhao [a,b], Xuan Liu [a,b], Caixia Liang [a,b], Youcai Zhu [a,b], Ziang Zhang [a,b], Kuang Yang [a,b]

[a] College of Environmental Science and Engineering, Hunan University, Changsha 410082, PR China
[b] Key Laboratory of Environmental Biology and Pollution Control (Hunan University), Ministry of Education, Changsha 410082, PR China

ARTICLE INFO

Article history:
Received 13 February 2022
Accepted 25 July 2022

Keywords:
Volatile organic compounds (VOCs)
Layered double hydroxides (LDHs)
Photocatalytic oxidation
Thermal catalytic oxidation
Gas components effects

ABSTRACT

Volatile organic compounds (VOCs) have received increasing attention for their severe hazards to the ecological environment and human health. Accordingly, various VOCs abatement technologies have been developed, where the selection of efficient catalysts is particularly critical. In recent years, the research of layered double hydroxides (LDHs)-based materials as novel catalysts has become one of the most attractive topics. With the tunability of LDHs in chemical composition, electronic structure and morphology, as well as their unique structural features and superior physicochemical properties, LDHs-based catalysts show enormous potential for environmental applications. This paper reviews the recent advances of LDHs-based materials for gaseous VOCs abatement, mainly covers two fields: photocatalytic oxidation and thermal catalytic oxidation. Especially, we summarize and compare the catalytic performance and intensified mechanisms of various LDHs-based materials, where the mechanistic details that lead to their varying results in terms of catalytic activity and reaction routes are the main focus of the discussion. Moreover, the effect of different gas components (e.g., SO_2, H_2O, CO, NO_x) on the performance of LDHs-based materials is examined. Our group also overviews the application of LDHs-based materials for VOCs adsorption, sensing and steam reforming. Finally, we provide an outlook on the current challenges and development strategies from the perspective of practical applications.

Contents

Abbreviations: VOCs, volatile organic compounds; LDHs, layered double hydroxides; MMO, mixed metal oxides; VB, valence band; CB, conduction band; ROS, reactive oxygen species; ESR, electron spin resonance; PL, photoluminescence; DFT, density functional theory; NPs, nanoparticles; LSPR, localized surface plasmon resonance; TRPL, time−resolved photoluminescence; GO, graphene oxides; BIEF, built−in electric field; LDO, layered double oxides; rGO, reduced graphene oxide; H_2−TPR, H_2−temperature programmed reduction; AC, auto−combustion; CP, co−precipitation; O_2−TPD, O_2−temperature programmed desorption; NH_3−SCR, NH_3−selective catalytic reduction; FT−IR, Fourier transform infrared; RH, relative humidity.

* Corresponding author at: College of Environmental Science and Engineering, Hunan University, Changsha 410082, PR China..
E-mail address: ctli@hnu.edu.cn (C. Li).

https://doi.org/10.1016/j.ccr.2022.214738
0010-8545/

1. Introduction

Volatile organic compounds (VOCs) are a major group of carbon-based chemicals with a boiling point below 250 °C under atmospheric pressure (101.325 kPa) [1]. Typically, they exhibit relatively high vapor pressure and low water solubility, which makes them susceptible to evaporate at normal temperatures (293.15 K) [2,3]. Most VOCs have been listed as major contributors to air pollution for long periods, especially the most common hazardous VOCs, including formaldehyde, benzene, toluene, propylene, phenol and acetone [4]. In general, the type and nature of VOCs depend on the source of emissions, while their impact on the atmosphere varies by their property and concentration [5–7]. These hazardous VOCs, not only directly as toxic and carcinogenic substances, but also indirectly as precursors to ozone/photochemical smog [8–10], cause severe harm to the ecological environment and human health [11,12]. What's worse, as the urbanization and industrialization continue to accelerate in the 21st century, the emissions of VOCs are increasing annually [13]. Between 1980 and 2010, the industrial emissions of non-methane VOCs in China increased by 11.6 times [14]. To reduce the adverse effect of VOCs pollutants, it is crucial to adopt effective and applicable actions.

Recently, strict regulations have been issued worldwide to limit the emissions of VOCs [12], and many end-of-pipe technologies are developed to abate VOCs, which can be divided into two types: recovery and destruction [15,16]. Recovery technologies (adsorption, condensation, and membrane separation) primarily involve the transfer of hazardous VOCs to another phase through physical and/or chemical interactions. The destruction methods (thermal incineration, biodegradation, thermal catalytic oxidation, photocatalytic oxidation, and non-thermal plasma oxidation) are mainly applied to oxidize toxic VOCs molecules to non-toxic products (e.g., CO_2, H_2O), where the photo/thermal catalytic oxidation is the dominant technique to treat dilute VOCs (<0.5 vol%) streams [2,17]. However, due to complex environmental conditions (the presence of multiple gas components) of VOCs emission sources and the varying nature of VOCs molecules, the photo/thermal catalytic oxidation of VOCs is often limited by the removal efficiency, product selectivity, durability and recyclability in the practical application [18,19]. Thus, the selection of effective catalysts becomes essential. Currently, the common catalysts can be classified into three main categories: (i) noble metal catalysts, (ii) non-noble metal catalysts, (iii) mixed-metal catalysts [7,20]. Noble metals (Pt, Pd, Au, Rh, Ag, etc.) are attractive by their excellent activity in VOCs oxidation, but they are generally expensive and prone to inactivation by sintering or poisoning [11]. Sometimes they don't have sufficient selectivity and stability [2,21]. Non-noble metal catalysts are mainly transition metal oxides and rare earth metal oxides (e.g., TiO_2, CuO, MnO_2, Fe_2O_3, CeO_2, Co_3O_4), they have been extensively researched for their availability and low cost [22,23]. Nevertheless, they possess lower efficiency and durability than noble metals-based catalysts in VOCs oxidation [24]. Mixed-metal oxides tend to be more reactive by combining multiple oxides to form a synergistic effect, such as Cu-Ce oxides [22], Mn-Ce oxides [25], Mn-Co oxides [26], and Mn-Ti oxides [27]. However, due to the uneven active site and low surface area, their activity and stability still remain to be improved [28,29]. Accordingly, a readily available, efficient and stable catalyst is the goal that researchers have been pursuing.

Layered double hydroxides (LDHs), also known as hydrotalcite-like compounds, are mostly synthetic materials with superior properties, such as tunable composition, large surface area, uniform metal dispersion, structural memory effect, low cost, thermal stability, and recyclability [30–33]. Recently, LDHs have developed rapidly in some important fields, including medicine [34,35], energy engineering [36], and environmental remediation [37]. In the photo/thermal catalytic oxidation of VOCs, LDHs also present attractive advantages compared to other conventional catalysts: (i) LDHs are facile to synthesize (e.g., simple aqueous co-precipitation method), and their structure, composition, as well as electronic, chemical properties can be readily designed for specific reactions and operating situations [38,39]; (ii) LDHs contain abundant surface functional hydroxyl groups, which significantly promote the adsorption and activation of VOCs molecules, and the tunable surface basicity also enables LDHs to be superior solid base catalysts [40,41]; (iii) the layered structure with large surface area and finely controlled chemical composition of LDHs facilitate the dispersion and modulation of active sites, which underlies the promising catalytic performance of LDHs-based catalysts [42]; (iv) their strong adsorption capacity of H_2O and O_2 molecules, the conversion between surface hydroxyl groups and reactive hydroxyl radicals, tunable band gap and broad optical response spectrum benefit the optimization of photocatalytic pathways [43]; (V) the structural tunability and the versatility of LDHs enable researchers to further improve the catalytic activity and stability of LDHs catalysts through various optimization strategies (e.g., support, assembly, modification, and topotactic transformation) [44,45]. Based on the above, LDHs-based materials are expected as novel catalysts with simultaneously improved activity, selectivity and stability. The rational design of efficient LDHs-based catalysts is of enormous interest in the research of photo/thermal catalytic oxidation of VOCs.

LDHs-based materials are being extensively explored for environmental remediation, some excellent reviews on the preparation, properties, and catalytic applications of LDHs-based materials have been published by different groups [43,46–49]. However, there are few reviews that focus on the catalytic performance of LDHs-based materials for VOCs abatement. Within the last decade, only Chen and co-workers concluded the recent

advances of mixed metal oxides (MMO) derived from LDHs for the heterogeneous catalytic oxidation of VOCs [50]. It is incomplete in providing a thorough overview of LDHs-based materials, the rapid growth of LDHs-based materials in VOCs abatement also requires an up-to-date and more comprehensive assessment. Hence, we summarize the recent advances of various LDHs-based materials, and attempt to illustrate their intensified mechanisms in photo/thermal catalytic oxidation of VOCs. In particular, the structure-activity correlation and the comparison of strengths and weaknesses in different LDHs-based catalysts are highlighted to provide a reference for the improvement of LDHs-based materials. Furthermore, the effect of typical gas components (e.g., SO_2, H_2S, H_2O, CO, NO_x) on catalytic performance is further explored. Our group also overviews the applications of LDHs-based materials for VOCs adsorption, sensing and steam reforming. Finally, the current technical challenges and development strategies are discussed from the perspective of practical applications. We hope this review will benefit the researchers interested in LDHs-based materials for VOCs abatement and encourage future works in this exciting field.

2. Overview of LDHs

LDHs are a group of versatile two-dimensional (2D) inorganic materials that can be expressed by the generic formula: $\left[M^{2+}_{1-x}M^{3+}_{x}(OH)_2\right]^{x+}\left[A_{x/n}\right]^{n-}\cdot mH_2O$, as shown in Fig. 1, where M^{2+} (e.g., Zn^{2+}, Mg^{2+}, Cu^{2+}, Co^{2+} or Ni^{2+}) and M^{3+} (e.g., Fe^{3+}, Al^{3+}, Cr^{3+} or Ga^{3+}) are divalent and trivalent cations with cation radius similar in size to Mg^{2+}, respectively [51]. Typically, the divalent metal cations are octahedrally coordinated with hydroxyl groups, and part of them can be substituted isomorphously by trivalent metal cations to form a positively charged layer, also known as the backbone of LDHs [52,53]. The x is the molar ratio of $M^{3+}/(M^{2+}+M^{3+})$, which ranges from 0.2-0.33 can be obtained as a pure hydrotalcite phase, and the M^{2+}/M^{3+} ratio of 2–4 is reasonably stable [54,55]. If the above x values are changed, other compounds with different structures will be generated [56–58]. With the octahedral structure of LDHs themselves, metal ions can be well dispersed in the cation layer, which may facilitate their performance in catalytic reactions [59,60]. The A^{n-} in the interlayer region is an exchangeable charge-balancing anion, which can be any charge-compensating anions, such as organic, inorganic, and complex heteropoly anions, maintaining the charge neutrality and stability of LDHs [61]. As known, the cationic layers of LDHs are not cross-linked, which enables the interlayer spacing to be expanded or reduced to contain a large area of interlayer anions. Therefore, the thickness of the cationic layer of LDHs is dictated by the chemical properties of the metal cations, while the spacing between the layers is determined by the size of the anions. The m is the number of sites occupied by water molecules in the interlayer region without anions [62]. Interestingly, each of the hydroxyl groups in the LDHs layer is orientated towards the interlayer region, and may form into hydrogen bonds with the interlayer anions and water molecules [52].

In most cases, the structure of LDHs is relatively stable. The desired modulation of the chemical property and valence state of the metal cations will not drastically change the backbone of LDHs. On this basis, exploiting the wide tunability of metal cation type, the M^{2+}/M^{3+} molar ratio, and the nature of the interlayer compensating anion, various LDHs materials with superior properties can be synthesized through artificial adjustment. Additionally, as inorganic mesoporous materials with pore sizes between 2 and 50 nm, LDHs can be restructured while sustaining their high surface to volume ratio (>100 m^2/g) [63], which further improves the functionality of LDHs. Moreover, the tunable composition and flexible structure of LDHs enable them to enhance the active sites and promote the catalytic performance through various optimization strategies, showing great potential in environmental remediation [49,64]. The topological transformation of LDHs precursors to mixed metal oxides (MMO) after calcination can further refine

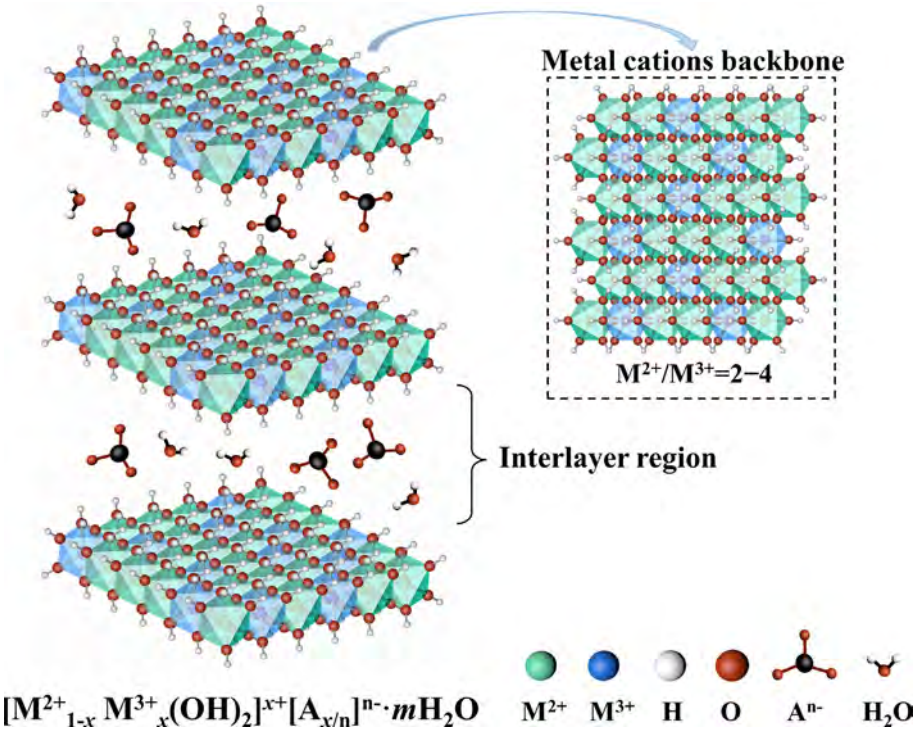

Fig. 1. The three-dimensional ideal crystal structure of LDHs displays the stacked metal hydroxide octahedra, with water and anions present in the interlayer region.

the structure modification strategy, and expand the application range of LDHs materials [65]. Recently, the scope of research on LDHs has extended from simple bicationic materials such as MgAl-LDHs to various LDHs composites (e.g., supported LDHs, assembled LDHs, modified LDHs, core-shell structured LDHs) and LDHs derivatives (e.g., MMO) in the photo/thermal catalytic oxidation of VOCs. These LDHs-based catalysts exhibited excellent catalytic performance, which will be discussed in detail below (Section 3 and Section 4).

3. LDHs-based materials for photocatalytic oxidation of VOCs

Photocatalytic technology emerged in the 1980s and matured with the gradual development of research on conventional TiO_2 photocatalysts [18,66]. The conversion of solar energy into chemical energy by the photocatalytic process is one of the most important fields for solving global energy problems [67]. In a typical photocatalytic oxidation reaction, when the incident photon energy is greater than the bandgap of photocatalysts, the electron (e^-) in the valence band (VB) can be excited into the conduction band (CB), leaving an oxidative hole (h^+) in the VB. Furthermore, h^+ and e^- will be further trapped by free H_2O and O_2 from the gas mixture to generate hydroxyl radicals ($\cdot OH$) and superoxide radicals ($\cdot O_2^-$), respectively [18]. These reactive oxygen species (ROS) are crucial for the catalytic reaction, which can oxidize pollutant molecules to H_2O and CO_2. However, most electron-hole ($e^- - h^+$) pairs are subject to the radiative or non-radiative recombination, leading to photoemission or heat, which reduces the photocatalytic efficiency [68]. Besides, the deactivation (e.g., SO_4^{2-} and S poisoning) and low efficiency (especially under visible light) of conventional photocatalysts have also been issues to be tackled [69,70]. Comparatively, the inherent superior property of LDHs and their structural tunability at the microscopic scale provide the vast prospect for the preparation of LDHs-based photocatalysts with desirable performance.

3.1. Virgin LDHs as photocatalysts

The unique photocatalytic property of virgin LDHs has been neglected for a long time, they are adopted for the photocatalytic oxidation of organic pollutants until the early 21st century [71,72]. The surprising catalytic performance of LDHs has attracted great attention from researchers and facilitated their rapid development. Concerning the VOCs abatement, virgin LDHs exhibit tremendous excellence over conventional TiO_2.

As the essential sources of highly reactive radicals in the photocatalytic process, the adsorption of H_2O and O_2 molecules on the surface of photocatalysts has a significant impact on their performance. The abundant surface hydroxyl groups of LDHs were confirmed to favor the adsorption process of H_2O and O_2 [73–75]. Fig. 2a showed the difference in adsorption parameters between the conventional TiO_2 (P25) and ZnTi-LDHs (ZT-LDHs) [76]. It was found that the H_2O and O_2 adsorption energy (E_{ads}, the absolute value) of ZT-LDHs was much higher than P25, while the adsorption of O_2 on P25 cannot proceed spontaneously (the value is positive). Furthermore, the bond length of the O_2 adsorbed on the surface of ZT-LDHs was obviously elongated, which contributed to the formation of $\cdot O_2^-$ radicals. It was consistent with the electron spin resonance (ESR) results in Fig. 2b. Similarly, Zou et al.[77] confirmed the generation of $\cdot O_2^-$ on ZnTi-LDHs by a simulated *in situ* ESR technique, and they speculated that $\cdot O_2^-$ radicals were induced by the transfer of photogenerated electrons from the surface of ZnTi-LDHs to the trapped O_2 molecules. In addition, as shown in Fig. 2c, Lv et al.[78] confirmed the abundant hydroxyl groups of LDHs could provide potential ·OH through trapping the photoexcited holes by the $AgNO_3$ content-dependent photoluminescence (PL) spectra (the sample was illuminated in the OH^-/H_2O-free acetonitrile solution). It implied that the surface hydroxyl groups of LDHs, which are abundant, fully exposed, and dynamically replenishable by free H_2O, had also played an essential role in the photocatalytic oxidation of VOCs. Most VOCs contain electron-rich structures, such as aromatic rings and oxygen-

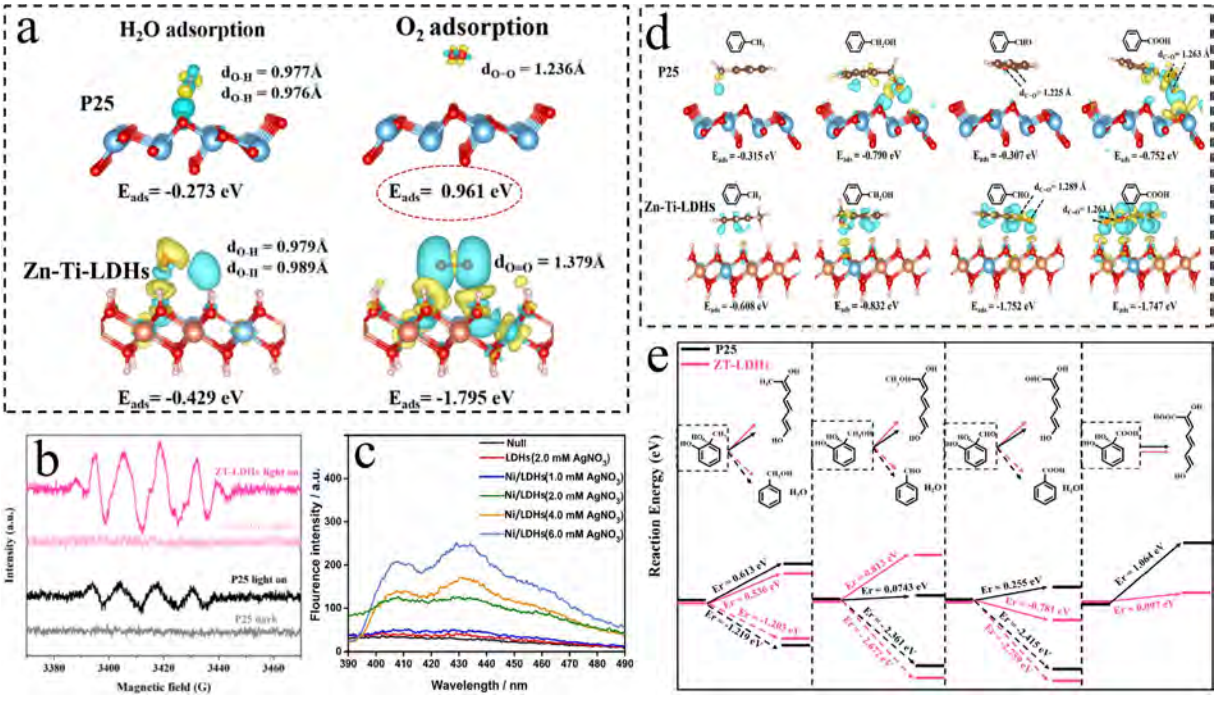

Fig. 2. (a) The simulated adsorption processes of O_2 and H_2O by DFT [76]. (b) ESR spectra in the dark and under UV light for superoxide radicals [76]. (c) $AgNO_3$ content-dependent PL spectra of Ni/LDHs [78]. (d) Adsorption energy and difference charge density of intermediates and (e) reaction energy (E_r) on P25 and ZnTi-LDHs by DFT [76].

containing functional groups, making them more susceptible to further oxidation by binding to ·OH [79,80]. It can be concluded that LDHs have a strong adsorption capacity for free H_2O and O_2, and their surface structure is more favorable for electron transfer, which leads to the efficient production of $\cdot O_2^-$ and ·OH radicals.

Based on these properties, LDHs tend to have more superior performance in photocatalytic oxidation of VOCs. For example, Liu et al. [76] achieved 75.2 % removal of toluene on ZT-LDHs compared to 10.9 % on P25 under UV irradiation. Notably, they found that fewer intermediates (benzyl alcohol, benzaldehyde and benzoic acid) were accumulated on LDHs. It was revealed by density functional theory (DFT) calculation (Fig. 2d) that the E_{ads} of these intermediates on ZT-LDHs was significantly higher, indicating the intermediates had a stronger interaction with the surface of ZT-LDHs, which was favored for the further oxidation. There was also strong covalent interaction between the O in the C═O of intermediates and the H in the surface hydroxyl groups of LDHs, enabling better adsorption and activation. The energy required (E_r) for the ring-opening reaction of intermediates further verified this. As shown in Fig. 2e, the E_r of typical intermediates (benzaldehyde, benzoic acid) on ZT-LDHs was much lower than P25, which indicated that the ring-opening reactions were more readily occurring on ZT-LDHs. In contrast, benzaldehyde on the P25 surface was more readily converted to benzoic acid, and produced a large accumulation of intermediates, which would lead to the deactivation of catalysts eventually.

In short, virgin LDHs possess a strong adsorption capacity for free H_2O and O_2, contributing to the generation of reactive radicals. The abundant hydroxyl groups on their surface not only facilitate the adsorption and activation of VOCs molecules, but also tend to be converted into reactive·OH. However, the photocatalytic performance by virgin LDHs under laboratory conditions seem to be unsatisfactory due to their wide bandgap, fast $e^- - h^+$ pairs recombination, and weak light absorption capacity [81–83]. As an example, Zhang et al. reported [84] a only 23.3 % removal of toluene on ZnAl-LDHs under visible light. Therefore, different optimization strategies have been proposed to further improve the catalytic performance of LDHs [85,86], which will be described in the following sections.

3.2. LDHs composites as photocatalysts

One of the effective strategies to improve their photocatalytic performance is to form composites by compounding the virgin LDHs with other functional units. Our group broadly classified LDHs-based composites into the following categories to review their respective applications in VOCs abatement: (i) supported LDHs, (ii) assembled LDHs, (iii) modified LDHs, (iv) core-shell structured LDHs. The supported LDHs employ LDHs as substrates, and disperse noble metals, metal oxides, or non-metallic on their layered structure. The assembled LDHs are multifunctional composites obtained by hybridizing LDHs with some other materials possessing complementary properties. The modified LDHs are usually prepared by introducing other metal or non-metal elements into the interlayer of LDHs, to improve their band structure and induce the formation of oxygen vacancies. As for the core-shell structured LDHs, metal oxides are used as the core, while LDHs are grown outside the metal core and act as the shell. They exhibit remarkable interfacial effects and generally result in the formation of core/shell heterojunctions, which contribute to better catalytic performance [87].

3.2.1. Supported LDHs photocatalysts

Nanoparticles (NPs) have extraordinary advantages over their bulk counterparts [88], especially the noble metal NPs are usually act as highly active centers. However, they are small and in a state of thermodynamic instability, thus rendering NPs prone to aggregation, sintering and even deactivation during reactions [89]. Immobilization of NPs on suitable supports is one of the effective ways to solve this issue.

LDHs have been proven to be promising supports for the immobilization and dispersion of various metal NPs owing to their unique layered structure, excellent adsorption capacity, and abundant surface hydroxyl groups [45]. In the field of VOCs abatement, the supported LDHs is the most frequently studied form of LDHs-based photocatalysts [43]. On the one hand, as supports of noble metal NPs, LDHs can prevent the aggregation/sintering through the external confinement effect of the LDHs layer, thus ensuring the high dispersion of noble metal NPs [42]. Some noble metals supported on LDHs usually exhibit strong support-determined morphology and size characteristics [90]. For instance, Zhang et al.[91] had confirmed that the crystallographic property of LDHs played an essential role in the position and particle size of the supported Au NPs. Li et al.[92] also suggested that there was a synergistic interaction between Au and LDHs that resulted in the homogeneous dispersion of Au NPs on the LDHs surface. Moreover, Lee et al.[93] proved that the abundant hydroxyl groups on LDHs stabilized the Pt NPs successfully and promoted the rapid diffusion of the reactants onto the surface of catalysts. As a result, the unique property of LDHs leads to smaller particle sizes and more uniform dispersion of noble metals supported on LDHs, which are considered to be one of the critical factors for improving catalyst activity and selectivity.

On the other hand, the metal cations (Co^{2+}, Ni^{2+}, etc.) in the LDHs host layer can also act as active sites that interact with the supported metal NPs, thus exhibiting a facilitation effect. Zou et al. [94] reported that Co mainly contributed to the catalytic activity over ZnCo-LDHs, while Zn provided structural support and/or synergistic effects. By supporting Au NPs on M_3Al-LDHs (M = Mg, Ni, Co), Li et al.[92] suggested that the presence of transition metals (Ni^{2+}, Co^{2+}) contributed to the catalytic activity. It was firmed that LDHs can also act as a co-catalyst for the catalytic reaction, not only as a support. Based on the above results, supporting noble metals on LDHs is a promising option. To date, a great number of studies have been done.

As mentioned in section 3.1, the photocatalytic activity of virgin LDHs is commonly limited to the weak light absorption capacity and fast recombination of $e^- - h^+$ pairs [95,96]. By contrast, a study by Katsumata et al.[97] showed that noble metals (Pt, Pd, Au) supported on ZnCr-LDHs significantly blocked the recombination of $e^- - h^+$ pairs through the efficient electron transfer from LDHs to noble metal NPs due to the lower Fermi level of noble metals. Moreover, the interaction between noble metals and LDHs contributed to the formation of heterojunctions, which was beneficial for the photocatalytic behavior. For example, the Schottky barrier formed by Ag and LDHs over Ag/ZnAl-LDHs was reported to adsorb resonant photons effectively [98], and the tight heterostructure between Pt and LDHs was also shown to greatly improve the catalytic activity under visible light by Li et al. [99]. It was of great implication for VOCs photodegradation under visible light or even near-infrared light. Recently, as displayed in Fig. 3a and 3b, Zhang et al. [84] proved that the visible light absorption (mainly 500–600 nm) of ZnAl-LDHs was significantly enhanced with Au supporting (from<4.0 % to 49.5 %). The same conclusion was obtained in the photocatalytic gaseous o-xylene experiments on Au/ ZnCr-LDHs by Fu et al. [85]. It is concluded that the strong localized surface plasmon resonance (LSPR) effect of noble metals plays an important role, which refers to the strong light absorption effect produced when the incident photon frequency matches the overall vibrational frequency of the noble metal NPs or metal conduction electrons [100]. In addition, the conduction electrons of the noble

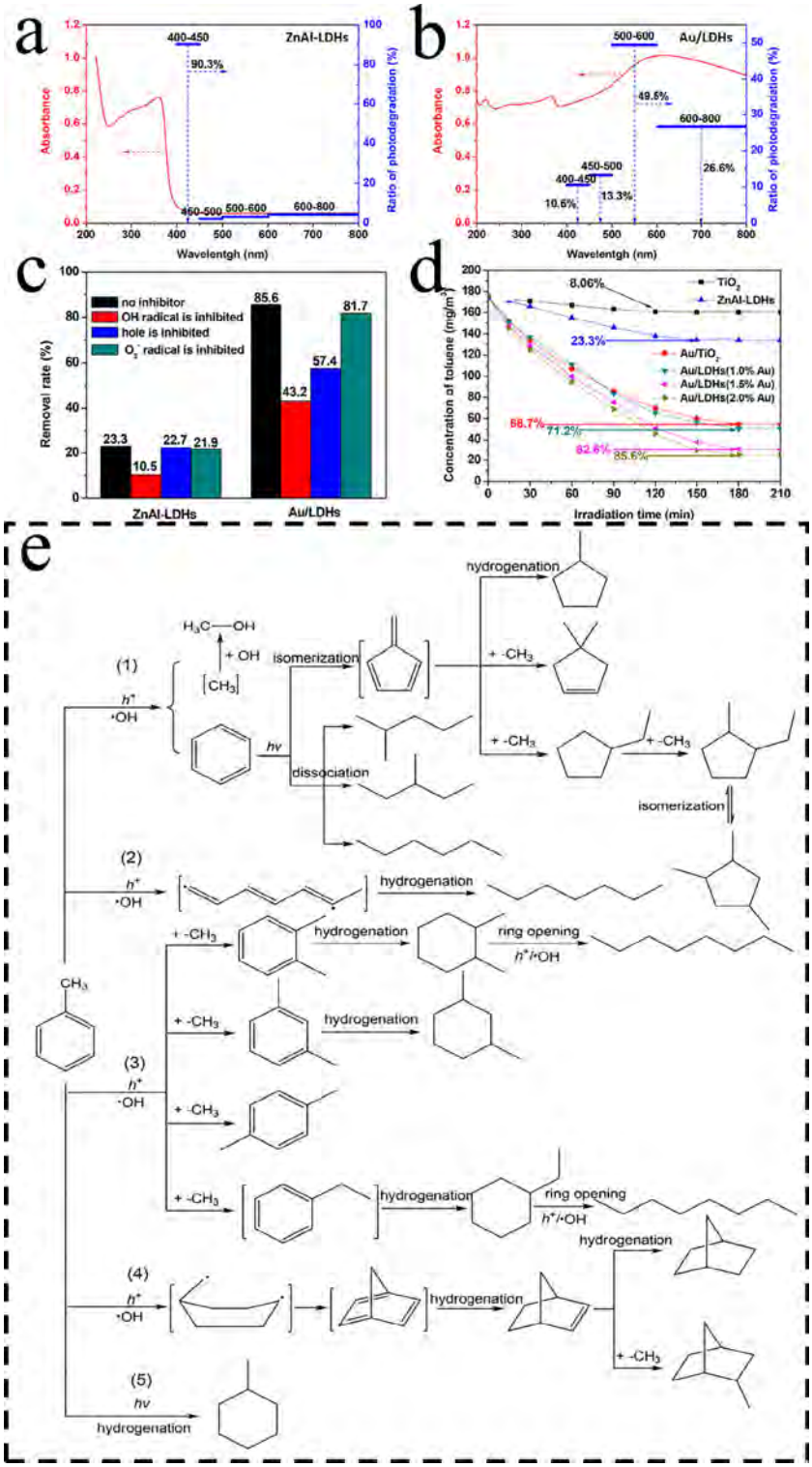

Fig. 3. (a) ZnAl-LDHs and (b) Au/LDHs photodegradation dependence on different wavelength ranges of visible light. (c) Toluene photodegradation without inhibitor and with inhibitor added. (d) The concentration of toluene versus irradiation time. (e) Intermediates and photodegradation pathways of toluene [84].

metal NPs receive the energy of the incident light through the LSPR effect and generate energetic electrons on the surface. These photoexcited electrons can activate the VOCs molecules adsorbed on the surface of catalysts and promote the reaction [101]. Notably, as shown in Fig. 3c, the dominant driving force for the photocatalytic reaction of ZnAl-LDHs was proved to be simply the hydroxyl radicals, while that of Au/ZnAl-LDHs (Au/LDHs) was simultaneously the holes and the hydroxyl radicals. As a result, the photocatalytic activity of toluene on Au/LDHs under visible light increased from the unsupported 23.3 % to 85.6 % (Fig. 3d). Moreover, as presented in Fig. 3e, photocatalytic oxidation of toluene over Au/LDHs is a complex reaction with various reaction pathways and numerous intermediates, which was consistent with the researches of Fu et al. [85]. Interestingly, the authors also investigated different

influencing factors in photocatalytic oxidation of VOCs, including initial toluene concentration, irradiation intensity, catalyst dose, reaction temperature and relative humidity. It is of great reference for realizing industrial application of the supported LDHs.

Overall, LDHs with promising stability, as excellent supports, not only can effectively immobilize and disperse small noble metal NPs (e.g., 4–12 nm Au NPs [84]), but also contribute numerous water molecules and hydroxyl groups within the structure, which are necessary for the production of ·OH radicals in the photocatalytic oxidation of VOCs [102]. In addition, noble metal NPs supported on LDHs can act as acceptors for electrons, accelerating the migration of photogenerated carriers on the surface of catalysts, thereby effectively inhibiting the recombination e^-–h^+ pairs and increasing their lifetime. It not only makes more e^- and h^+ involved in the generation of reactive radicals, but the h^+ have more access to participate independently in the oxidation reaction of VOCs. Combined with the enhancement in the absorption of visible light by the LSPR effect of noble metals, the photocatalytic performance of supported LDHs will be greatly enhanced eventually.

3.2.2. Assembled LDHs photocatalysts

Assembly of LDHs with other semiconductors is another effective way to utilize their synergistic effects fully [103]. As we know, LDHs have been widely used as a basic framework for the fabrication of various multifunctional hybrids due to their properties such as natural enrichment, high adsorption capacity, outstanding stability, and abundance of surface hydroxyl groups [72,104]. Accordingly, assembling some other materials with complementary photocatalytic properties with LDHs can also improve the separation and migration efficiency of photogenerated carriers, thus optimizing the photocatalytic process.

For example, the conventional TiO_2 could be assembled with MgAl-LDHs and exhibited synergistic effects, which significantly improved the separation of e^-–h^+ pairs and generated abundant reactive radicals at the TiO_2/LDHs interface [105]. Hence, it achieved a degradation efficiency of 91.7 % for toluene under real sunlight irradiation. Chen et al.[83] also proposed a strategy to tune the electronic structure of LDHs. They prepared a novel heterojunction of α-Ga_2O_3/MgAl-LDHs with superior and stable photodegradation (90.71 %) and mineralization (84 %) of toluene. As displayed in Fig. 4a, a Ga—O—H channel for charge transfer was formed at the interface of MgAl-LDHs and α-Ga_2O_3. Under UV irradiation, the photogenerated electrons and holes were induced in α-Ga_2O_3, where the electrons were rapidly transferred to MgAl-LDHs (Fig. 4b), thus promoting the charge carrier separation. The local electron functions of α-Ga_2O_3/MgAl-LDHs (Fig. 4c) further confirmed it, the Ga, O, and H atoms exhibited a strong interaction to form the Ga—O—H structure, thereby constituting the transport channel of electrons. In addition, as essential sources of reactive radicals, the activation of O_2 and H_2O molecules on α-Ga_2O_3/MgAl-LDHs surface had also been investigated by DFT calculations. As displayed in Fig. 4d, differential charge density visualized the electronic interaction of O_2 with the surface of catalysts. The adsorption energy (E_{ads}) and transfer charge (Δq) of O_2 were -2.1 eV and 1.05 eV, respectively, which indicated that O_2 gained electrons. Combined with the extended bond length after adsorbing O_2 (from 1.21 Å to 1.41 Å), it was concluded that α-Ga_2O_3/MgAl-LDHs promoted the O_2 adsorption and activation to form bridging O—O bonds, making the charge transfer between the catalysts and O_2 more easily. In contrast, the insignificant change in bond length after adsorption (from 0.96 Å to 0.98 Å) and the low E_{ads} (−0.6 eV) suggested that H_2O had not achieved effective activation on the surface of MgAl-LDHs. It might be bound to the holes in α-Ga_2O_3. As shown in Fig. 4e, abundant ROS were produced on Ga_2O_3/MgAl-LDHs surface, and eventually mineralized the toluene.

Moreover, the assembly of LDHs with some layered nonmetallic materials to construct the hierarchically structured composites, also improves the functionality of catalysts, and further enhances the catalytic performance due to the synergistic effect. Nayak et al.[106] had synthesized a series of highly efficient g-C_3N_4/NiFe-LDHs photocatalysts by the impregnation method, the excellent photocatalytic activity was certificated by the significant quenching of the PL signal, and the extended photogenerated charge lifetime was also confirmed by time-resolved photoluminescence (TRPL) spectra. Similarly, via the in-situ growth method, Wu et al.[32] had developed a newly 2D-2D heterostructure com-

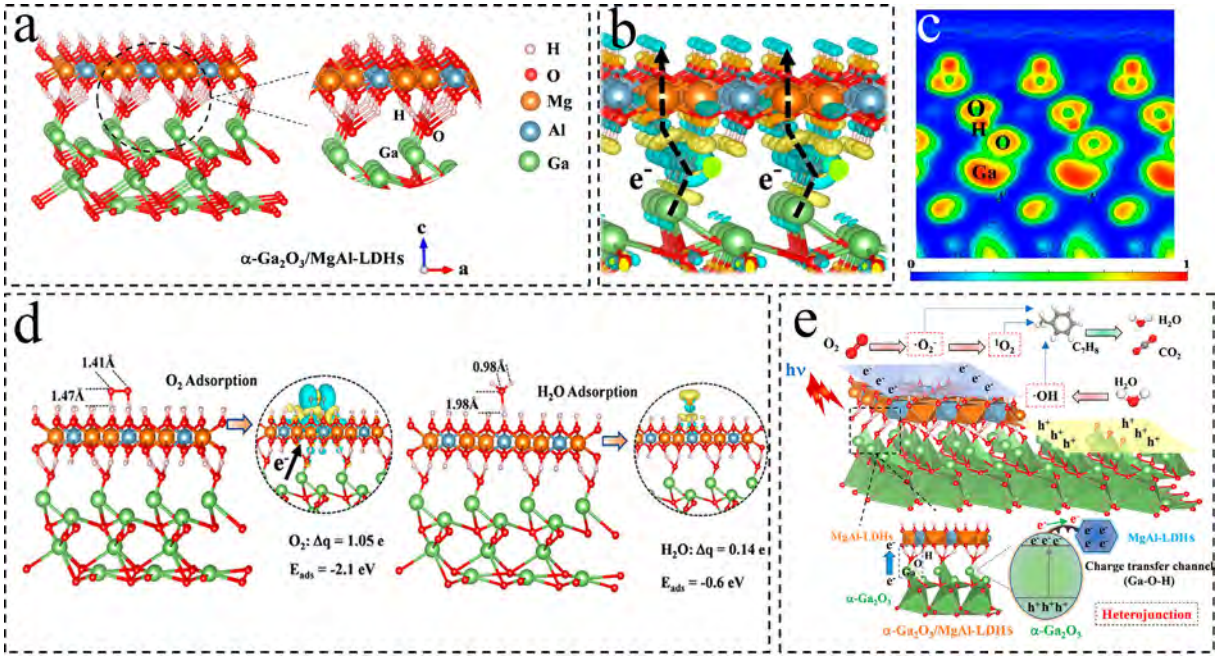

Fig. 4. (a) The optimized structure. (b) The differential charge density. (c) The local electron functions. (d) The O_2 and H_2O adsorption simulation. (e) Mechanism of toluene photodegradation of α-Ga_2O_3/MgAl-LDHs [83].

posed of oxygen-doped carbon nitride (OCN) and CoAl-LDHs, exhibiting significant visible-light absorption property and outstanding photogenerated e^-–h^+ pairs separation capability. The graphene oxides (GO) were also assembled with LDHs, and the prepared bifunctional catalysts also showed excellent catalytic performance [107]. Arguably, the assembly of LDHs with some layered non-metallic materials (e.g., C_3N_4, GO) has proven to be a promising and feasible direction, although it has not been reported in VOCs abatement.

3.2.3. Modified LDHs photocatalysts

The modification of LDHs is one of the effective methods to improve the structural characteristic and physicochemical property. LDHs can be directly modified by metals or non-metals. So far, there have been some attempts to introduce non-metallic elements (N, P, S, etc.) into LDHs. It is generally accepted that the introduction of these heteroatoms with strong electronegativity can serve to change their morphology and increase the charge carrier mobility [108,109]. For instance, Yang et al. [110] observed that the doping of P on NiCoZn-LDHs would result in a more regular morphology, which might provide more active sites. Guo et al. [111] found a modulating effect of S on the electronic structure of the active cations over the S-modified FeNi-LDHs, which facilitated the transfer of electrons.

Another research hotspot on modified LDHs is the partial substitution/doping of metal cations, which has also been verified to modify the morphology, band structure, and electronic property of LDHs. As an example, the morphological variations of LDHs-based materials were systematically investigated by modifying the divalent cations (Zn^{2+} was replaced by Cu^{2+}) and trivalent cations (Al^{3+} was replaced by Fe^{3+} or Ti^{4+}) within the LDHs sheets network (Fig. 5a-5c) by Seftel et al.[112]. It was found that the presence of Cu^{2+} led to a higher degree of agglomeration, while the partial replacement of Al^{3+} with Fe^{3+} and Ti^{4+} resulted in a significant reduction in the size of particles. In addition, as reported by Lv et al. [78], the replacing Mg^{2+} by Ni^{2+} might reduce the crystallinity and induce defective structure (generating oxygen vacancy) of LDHs. It was clear that the partial substitution of metal cations directly affects the microstructure of LDHs materials. What's more, it also plays a significant role in adjusting the band structure. As shown in Fig. 5d, the controlled Ni^{2+} substitution for Mg^{2+} in Mg_2Al-LDHs not only produced new absorption peaks at 377, 416, 645 and 745 nm, but also red-shifted the edge of the absorption band. Their band structures were presented in Fig. 5e, the VB was elevated, and CB was shifted in a valley-like mode with the change of Ni content, which indicated that the Ni^{2+} mainly contributed to the band structure of LDHs. The total electronic density of states (TDOS) by DFT in Fig. 5f further confirmed that the substitution of Ni^{2+} for Mg^{2+} shifted both CB and VB up (regions I and III), while the presence of oxygen vacancy (Ov) elevated VB (region I) and introduced a middle energy level (region II), simultaneously shifted CB down (region III).

Besides the band structure, the separation efficiency of e^-–h^+ pairs was also researched by Lv et al.[78]. The ns-level time-resolved fluorescence spectra (Fig. 5g) presented that the average lifetime of the charge carrier in Ni/LDHs was 5.64 ns, almost 2.5 times than LDHs (2.28 ns), which demonstrated that Ni^{2+} substitution promoted the e^-–h^+ separation. The DMPO-ESR spectra for $\cdot O_2^-$ (Fig. 5h) and ·OH (Fig. 5i) also suggested that the Ni/LDHs could generate more ROS. Notably, the Ni^{2+} was also proved to promote the conversion of surface hydroxyl groups to ·OH. As a result, the photocatalytic performance was greatly enhanced. It was consis-

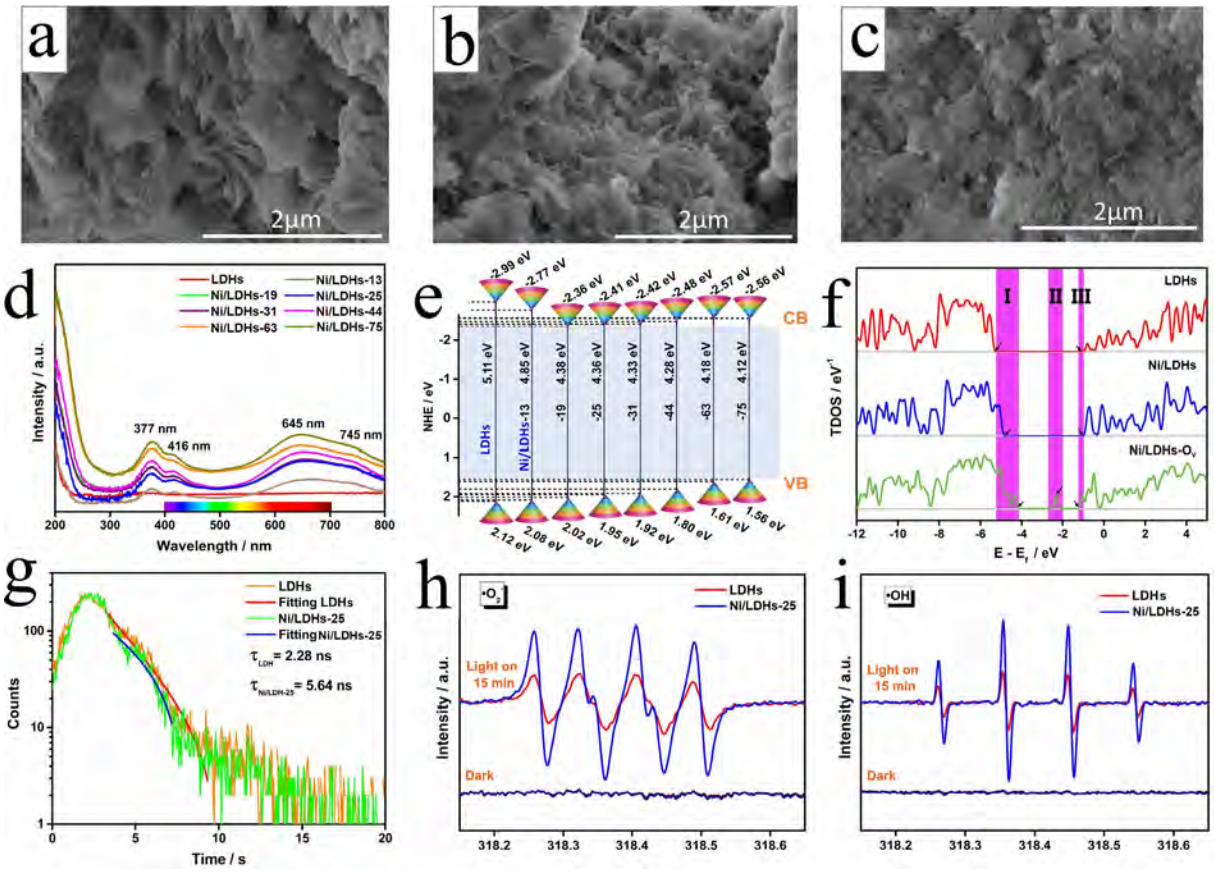

Fig. 5. SEM images of (a) ZnAl-LDH, (b) CuZnAl-LDHs, (c) CuZnFeTi-LDHs [112]. (d) UV-vis DRS spectra. (e) Band structures. (f) Total electronic density of states. (g) The ns-level time-resolved fluorescence spectra. The DMPO spin-trapping ESR spectra for (h) $\cdot O_2^-$ and (i) ·OH of LDHs and Ni/LDHs [78].

tent with the findings of Mendoza-Damián et al.[113] over the Sn^{4+} modified ZnAl-LDHs. In another report, the modification of Co was found to facilitate the deposition of Au on LDHs through strong electronic interaction, which promoted the adsorption and activation of O_2, thus contributing 96.2 % removal of formaldehyde over Au/Co-LDHs [114].

Recently, Zhang et al.[86] also confirmed the contribution of Mn substitution to the modulation of the band structure and the separation efficiency of photogenerated carriers. More importantly, Mn-substituted ZnAl-LDHs (MZA) was found to favor the formation of surface oxygen vacancy (Fig. 6a), which provided a deeper insight into the synergistic effect of metal substitution and oxygen vacancy. Interestingly, the MZA achieved the highest removal of 95.9 % for toluene, while the MZA-o (MZA without O vacancy, calcined under O_2 atmosphere) was only 87.4 %. It is reasonable to believe that, in addition to Mn substitution, oxygen vacancies contribute to the photocatalytic oxidation of VOCs in some way. As shown in Fig. 6b, the steady-state PL results corresponded to the photocatalytic activity, and MZA exhibited a lower recombination efficiency of $e^- - h^+$ pairs, which further confirmed that the superior photocatalytic performance of MZA was owed to the Mn substitution and more O vacancies. In addition, the DMPO-ESR results (Fig. 6c) suggested that MZA was much more capable of producing $\cdot O_2^-$ than others, while MZA-o was comparable to ZA (ZnAl-LDHs). It implied that the O vacancy was more responsible for the $\cdot O_2^-$ production than the Mn substitution, which was further confirmed by the DFT calculation. As displayed in Fig. 6e-6 g, MZA possessed greater surface adsorption energy (E_{ad}), and the O—O bond length of O_2 was apparently longer than that of MZA-o and ZA. It meant that the O vacancy not only contributed to capturing more O_2 and H_2O, but facilitated the weakening of O—O bond, which was more beneficial to the activation of O_2. Therefore, more ROS could be produced by the synergistic effect of Mn substitution and O vacancy, where oxygen vacancy played a more critical role.

In summary, the modification of LDHs by metal cations (e.g., Ni [78], Mn [86]) has a significant effect on the microstructure of LDHs, which not only the change in morphology (more regular), but also inducing surface defects (generating oxygen vacancies). More importantly, the modified LDHs can optimize the band structure, promote the separation of photogenerated carriers, and contribute to the massive generation of ROS. Notably, some metal cations (e.g., Mn [86]) has a significant synergistic effect on the metal substitution and oxygen vacancy. These effects greatly improve the photocatalytic oxidation capacity of LDHs, and it is highly promising for VOCs abatement.

3.2.4. Core-shell structured LDHs photocatalysts

It has been proposed that integrating LDHs with other materials having matched band structures to produce the core-shell structured catalysts. In this way, the directed charge flow with e^- and h^+ will be well controlled, thus improving the utilization efficiency of photogenerated carriers. Furthermore, core-shell structured LDHs photocatalysts exhibit a higher specific surface area and more active sites due to the unique layered structural characteristics of LDHs. It is widely used in various catalytic reactions [115,116], including the photocatalytic oxidation of VOCs.

In general, some metal oxides are used as the core, while LDHs are grown as shells outside the metal core to form multifunctional composites. For instance, the Cu_2O@ZnCr-LDHs core-shell structured photocatalysts (Fig. 7a) had been successfully synthesized by Wang et al.[115]. It was found that the Cu_2O@ZnCr-LDHs took full advantage of the synergistic effect of Cu_2O and ZnCr-LDHs via band structure control and interfacial chemical tuning (Fig. 7b), thus exhibiting a surprising catalytic activity under visible light. Xia et al.[117] had also employed the CeO_2@CoAl-LDHs core-shell structured catalysts for the photodegradation of some typical VOCs. In contrast to CoAl-LDHs (Fig. 7c), the CeO_2@CoAl-LDHs (Fig. 7d) exhibited a larger specific surface area (93 m^2/g) and narrower size distribution, which contributed to the more active sites. More importantly, a built-in electric field (BIEF) was found in the Z-scheme heterostructure of CeO_2@CoAl-LDHs (Fig. 7g), which facilitated the rapid flow of electrons from the CB of CeO_2 to the VB of LDHs. This electron transfer path effectively prevented the recombination of photogenerated $e^- - h^+$ pairs,

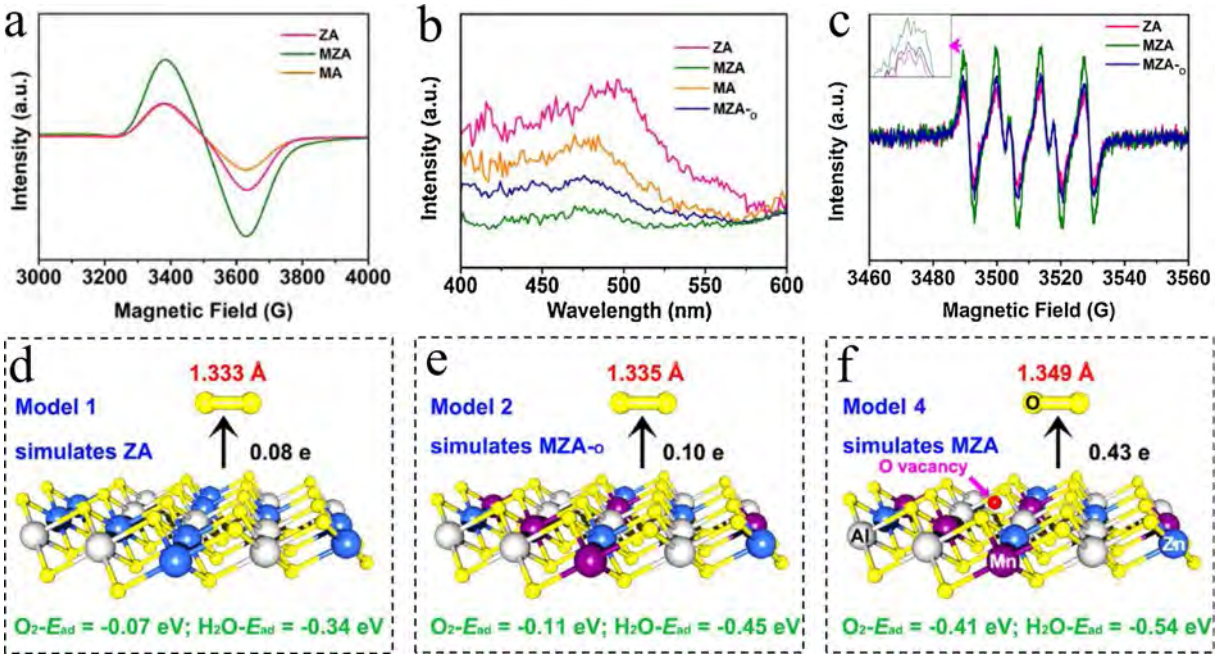

Fig. 6. (a) ESR spectra for O vacancy. (b) The steady-state PL spectral and (c) The DMPO-ESR spectra for $\cdot O_2^-$ of ZA (ZnAl-LDHs), MA (MnAl-LDHs), MZA (Mn-substituted ZnAl-LDHs), and MZA-o (MZA without O vacancy, calcined under O_2 atmosphere). Calculated O_2 and H_2O adsorption energy and O—O bond length of O_2 adsorbed on (d) ZA, (e) MZA-o, and (f) MZA [86].

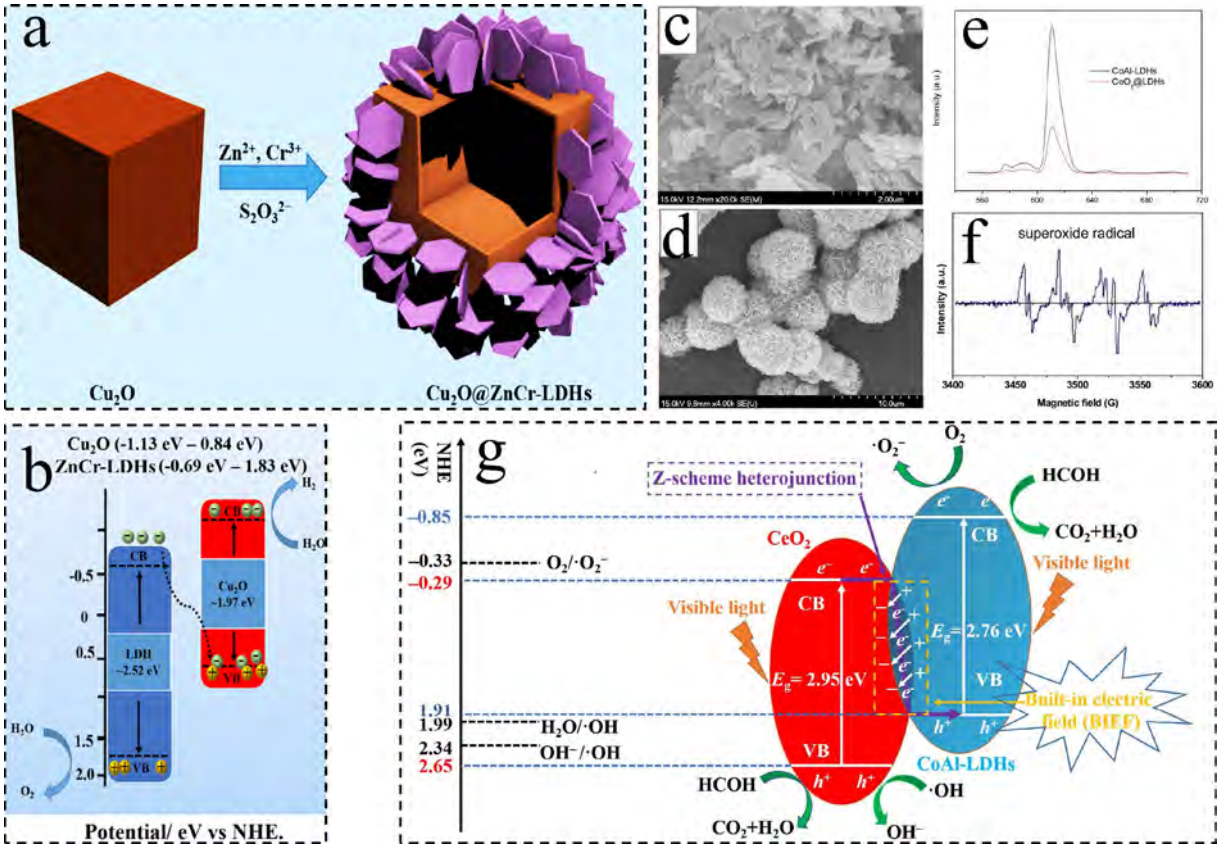

Fig. 7. Schematic illustration for (a) the preparation and (b) the band structure of Cu_2O@ZnCr-LDHs [115]. SEM images of (c) CoAl-LDHs and (d) CeO_2@CoAl-LDHs. (e) The PL spectroscopy. (f) The DMPO ESR spectra for $\cdot O_2^-$. (g) Photocatalysis mechanism of formaldehyde on CeO_2@LDHs [117].

which was confirmed by the PL spectroscopy (Fig. 7e). More catalytically active radicals were also generated substantially (e.g., the $\cdot O_2^-$ in Fig. 7f). As a result, the photocatalytic activity of CeO_2@-CoAl-LDHs for formaldehyde, benzene, toluene and xylene ranged from 76.7 % to 93.1 % under visible light. In addition, the effects of different factors on the photocatalytic activity of CeO_2@LDHs were investigated by the system kinetic analysis, which showed that the flow rate of VOCs molecules had the most significant effect, while the light intensity affected the least.

The strong interactions at the core-shell interface and the highly matchable band structures have shown great potential [118,119]. Moreover, their adjustable size, shape and compositional composition lead to the novel structural flexibility, stability and selectivity [43], deserving further investigation by researchers.

3.3. Summary and comparison of the strengths and weaknesses of typical LDHs-based photocatalysts

In conclusion, as for virgin LDHs, the strong adsorption capacity for H_2O and O_2 molecules contributes to the generation of reactive radicals, and the abundant hydroxyl groups on their surface not only facilitate the adsorption and activation of VOCs molecules, but also tend to be converted into reactive ·OH. There properties enable them to perform much better than conventional TiO_2 in the photocatalytic oxidation of VOCs. However, their wide bandgap, rapid recombination of photogenerated $e^- - h^+$ pairs, and weak light absorption limit their applications. Therefore, various optimization strategies (e.g., supported, assembled, modified, and constructed core–shell structure) were adopted to improve the performance of LDHs-based photocatalysts by virtue of the structural tunability and versatility of LDHs. For the refined design and synthesis of LDHs-based photocatalysts, Table 1 summarizes the typical photocatalysts for VOCs abatement and their intensified mechanisms.

Due to the LSPR effect of noble metal NPs, the absorption of visible light by supported LDHs is remarkably promoted, and noble metal NPs significantly reduces the recombination rate of $e^- - h^+$ pairs by accepting electrons from LDHs. Similarly, through combining the benefit of different desirable functional compositions, there are some other pathways to reduce the recombination of $e^- - h^+$ pairs and generate more reactive radicals, such as assembled LDHs constructed the electron transfer channels, modified LDHs improved the band structure and induced the formation of oxygen vacancies, core-shell structured LDHs formed the Z-scheme heterostructure with the built-in electric field. Additionally, the modified LDHs and core-shell structured LDHs will change the microstructure of LDHs (more regular), resulting in a larger specific surface area and more uniform size distribution, which may provide more active sites for reactions. In short, we compared their strengths and weaknesses (aspects for improvement) in Table 2. We hope that this information will help researchers design and develop efficient and stable LDHs-based photocatalysts for practical applications.

4. LDHs-based materials for thermal catalytic oxidation of VOCs

Thermal catalytic oxidation is gaining more attention as an effective and economically feasible technology for VOCs abatement, which is relatively eco-friendly due to its low operating temperature and no secondary pollution [121–123]. Different from photocatalytic oxidation technology, which relies on semiconductor-based photocatalysts that excite reactive radicals

Table 1
The summary of typical LDHs-based photocatalysts and their intensified mechanisms.

Materials	Type of LDHs	Synthesis methods	Experimental conditions	Catalytic activity	Intensified mechanisms	Ref.
ZnTi-LDHs	Virgin LDHs	Hydrothermal method	Catalyst: 0.2 g; light source and intensity: mercury lamp, 0.29 W/cm^2; flow rate: 100 mL/min	50 ppm toluene: 75.2 %	Activation of intermediates; improved surface electronic structure; more active radicals	[76]
Au/ZnCr-LDHs	Supported LDHs	Hydrothermal and wet precipitation method	Catalyst: 1.5 g; light source and intensity: xenon lamp, 0.5 W/cm^2; relative humidity: 50 %	175 mg/m^3 o–xylene: 83.6 %	More active radicals; enhanced visible light absorption; improved electron transfer efficiency	[85]
Au/ZnAl-LDHs	Supported LDHs	Hydrothermal and wet precipitation method	Catalyst: 2.0 g; light source and intensity: 500 W xenon lamp; relative humidity: 50 %	175 mg/m^3 toluene: 85.6 %	Enhanced visible light absorption; more active radicals; Reduced recombination of e^-–h^+ pairs	[84]
TiO_2@MgAl-LDHs	Assembled LDHs	Co-precipitation and in-situ hydrolysis method	Catalyst: 0.03 g; light source and intensity: 500 W xenon lamp	171.6 mg/m^3 toluene: 91.7 %	Facilitated separation of e^-–h^+ pairs; more active radicals	[105]
TiO_2/MgAl-LDHs	Assembled LDHs	Hydrothermal and solvothermal method	Catalyst: 0.4 g; light source and intensity: 300 W UV lamp; flow rate: 100 mL/min; relative humidity: 90 %	50 ppm toluene: 84.3 %	More hydroxyl radicals; improved H_2O adsorption behavior; abundant surface hydroxyl groups	[79]
α-Ga_2O_3/MgAl-LDHs	Assembled LDHs	Hydrothermal method	Catalyst: 0.1 g; light source and intensity: 300 W mercury lamp; flow rate: 1000 mL/min; Relative humidity: 50 %	50 ppm toluene: 90.7 %	Facilitated separation and transport of e^-–h^+ pairs; enhanced activation of O_2/H_2O molecules; abundant ROS; improved band structure	[83]
Ag/AgCl@TiO_2-LDHs	Modified LDHs	Hydrothermal and photoreduction method	Catalyst: 0.04 g; light source and intensity: 300 W xenon lamp	172.05 mg/m^3 toluene: 92 %	Sufficient surface hydroxyl ions; surface plasma resonance of Ag/AgCl; promoted the separation of e^-–h^+ pairs	[120]
Mn-substituted ZnAl-LDHs	Modified LDHs	Co-precipitation method	Catalyst: 0.5 g; light source and intensity: 300 W xenon lamp; humidity: 5 %	50 ppm toluene: 95.9 %	More surface oxygen vacancy; improved band structure; facilitated separation of e^-–h^+ pairs; enhanced adsorption and activation of O_2	[86]
CeO_2@CoAl-LDHs	Core-shell structured LDHs	Hydrothermal method	Catalyst: 10 g; light source and intensity: 400 W xenon lamp; flow rate: 1500 mL/min; relative humidity: 50 %	32.0 mg/m^3 formaldehyde, benzene, toluene: 86.9 %, 90.3 %,93.1 %	Narrower bandgap; larger specific surface area; More uniform size distribution; improved electron transfer efficiency and separation of e^-–h^+ pairs	[117]

Table 2
The comparison of strengths and aspects for improvement of various LDHs-based photocatalysts.

Type of LDHs	Strengths	Aspects for improvement
Virgin LDHs	Flexible structural tunability, extensive surface hydroxyl groups, great adsorption, stability and recyclability	Medium surface area, wide bandgap, fast e^-–h^+ pairs recombination and weak absorption intensity in UV-visible region
Supported LDHs	Strong support-determined morphology and size characteristic, more active reaction centers (noble metal NPs), high e^-–h^+ pairs separation and transportation efficiency, wide optical response window, great dispersion and adsorption	High cost of noble metals, poor adsorption efficiency, low surface area, low stability
Assembled LDHs	Improved electronic structure, high e^-–h^+ pairs separation and transportation efficiency, the synergistic effect between different components	Low surface area, narrow optical responsive window
Modified LDHs	Improved microstructure and band structure, more ROS, high e^-–h^+ pairs separation efficiency	Narrow optical responsive window, low stability
core-shell structured LDHs	Large specific surface area, high e^-–h^+ pairs separation and transportation efficiency, strong interaction at the core-shell interface, formation of heterojunctions, flexible structural tunability	Hard to synthesize, poor stability

under light irradiation, the reducibility of catalysts is the most critical aspect in thermal catalytic oxidation [24]. It usually involves the occurrence of a typical redox reaction (*Mars-van Krevelen* mechanism), where metal cations along with the activated lattice oxygen species (O^{2-}) will oxidize VOCs molecules to CO_2 and H_2O with the input of an external heat source. Nevertheless, developing efficient and stable thermocatalysts at low temperatures is still a challenging task. So far, LDHs have been widely applied in heterogeneous catalysis [45,52], and the versatility of LDHs-based materials (e.g., intercalation, delamination, topological transformation) has been extensively studied by researchers [42,124]. What's more, various catalytically active transition metals can be integrated into LDHs precursors [124]. These properties contribute to the high dispersion, great stability and excellent catalytic performance of LDHs-based materials in thermal catalytic oxidation of VOCs.

4.1. LDHs composites as thermocatalysts

LDHs have been extensively utilized as a basic framework for fabricating various multifunctional composites [72,104]. In the low-temperature catalytic oxidation of VOCs, the superior inherent properties of LDHs have also been deeply investigated. Recently, it

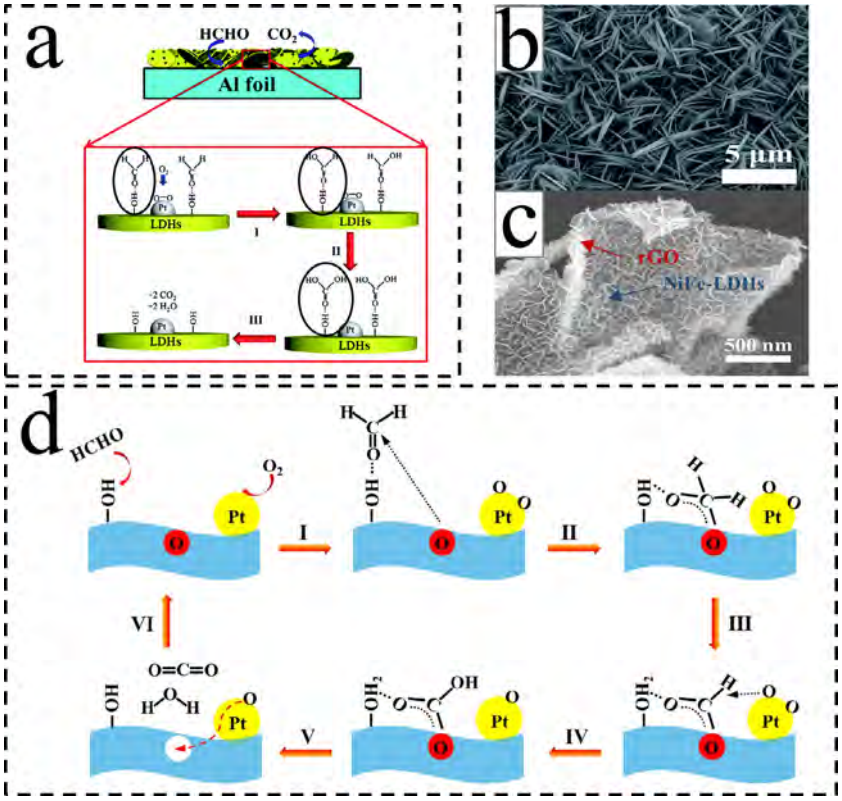

Fig. 8. (a) Suggested catalytic oxidation mechanism of HCHO and (b) SEM images of Pt/LDHs-Foil [128]. (c) SEM images and (d) reaction mechanism of HCHO oxidation on the Pt/NiFe-LDHs/rGO [40].

was reported that the surface hydroxyl groups of LDHs played a crucial role in the reactions [125–127]. As presented in Fig. 8a, Ye et al.[128] confirmed that the abundant hydroxyl groups on the surface of Pt/LDHs-Foil catalysts could function as adsorption centers for HCHO molecules, which was necessary for typical gas–solid catalytic reactions. Moreover, the hydroxyl groups could capture some intermediate products (e.g., formate species, carbonic acid) efficiently, thus promoting the oxidation reaction of HCHO significantly. Notably, the hierarchical porous structures of LDHs (Fig. 8b) could also facilitate oxidation reactions by reducing the diffusion resistance of gaseous reactants and products. It was also verified by Yan et al.[129], the Pt/NiAl-LDHs they prepared could completely mineralize HCHO at room temperature. Furthermore, by a calcination under N_2 atmosphere at 500 °C, Li et al.[114] converted Au/LDHs to Au/LDO (layered double oxides), while the HCHO catalytic activity of the latter was remarkable decreased due to the dehydroxylation. This is another evidence that surface hydroxyl groups are actively involved in the catalytic oxidation process of VOCs. In general, as shown in Fig. 8d, the crucial roles of surface hydroxyl groups of LDHs in HCHO oxidation are reflected in two aspects [40]: Firstly, connecting HCHO molecules through hydrogen bonds and enriching them on the surface of catalysts. Secondly, converting HCHO molecules into formate species, and further oxidizing them to unstable carbonic acid with the help of active oxygen species (generated by other active components, such as noble metal NPs). Eventually, these intermediate products are rapidly decomposed into CO_2 and H_2O.

The composite of some functional components with LDHs also provides a promising strategy for the low-temperature catalytic oxidation of VOCs. As shown in Fig. 8c, Wang et al.[40] successfully combined NiFe-LDHs with laminated reduced graphene oxide (rGO) to prepare Pt/NiFe-LDHs/rGO. With the incorporation of rGO, the LDHs composites exhibited the highest HCHO removal efficiency of 92.5 % within 60 min at room temperature. It was demonstrated that the unique hierarchical structural features of Pt/NiFe-LDHs/rGO provided a larger surface area, which resulted in abundant active sites and highly dispersed Pt NPs. In short, the abundant surface hydroxyl groups and unique layered structural properties enable LDHs to be favorable functional components, and various LDHs composites have shown substantial potential in low-temperature catalytic oxidation of VOCs.

4.2. Mixed metal oxides (MMO) thermocatalysts based on the topological transformation of LDHs

Recently, researchers have begun to recognize that the topological transformation can be performed to improve the catalytic performance by exploiting the existing edge and corner site with few coordinative unsaturated active sites of LDHs [130,131]. The derivatives obtained after a topological transformation process (commonly calcined) can inherit the structural characteristics of the LDHs precursor, resulting in uniformly dispersed metal cations. During the calcination process, the intense interaction between the active components and the simultaneously formed substrate prevents the aggregation/sintering of the metal particles, which improves their stability. Additionally, the highly porous MMO have a larger specific surface area of typically 100–300 $m^2 \cdot g^{-1}$ than the parent LDHs (40–120 $m^2 \cdot g^{-1}$) [132], which may contribute to providing more active sites for reactions. More importantly, MMO improved the reducibility due to the synergistic effect between each metal component. Therefore, LDHs derived MMO or LDO have reported to be prominent in thermal catalytic oxidation of VOCs [45,52,133].

In general, LDO is a part of MMO by structure [134], and there is no substantive difference between them (they are uniformly referred to as MMO for convenience in this paper). Through the

heat to certain temperatures, LDHs can convert readily to the corresponding derived MMO, which usually involves three steps: (1) dehydration, (2) crystallization of metal oxides, (3) decomposition of interlayer anions (e.g., hydroxyl, carbonate) and structural collapse [135,136]. Due to the tunable nature of cations in LDHs, various active transition metals (e.g., Cu, Fe, Co, Mn, Ni, Ti, and Zn) can be immobilized in the host layer [137–139]. The variation in the number of metal species (commonly one, two, or three) and the metal combinations contribute to the diversity of LDHs derivatives. Moreover, the synergistic effect between these active species led to better performance in thermal catalytic oxidation of VOCs [50]. Hence, MMO are the most commonly reported catalysts based on LDHs for the thermal catalytic oxidation of VOCs. Over the past decades, researchers have made remarkable progress. We will systematically discuss the effect of calcination temperature, synthesis method, metal ratio, and other factors on the catalytic performance of MMO in the following.

As mentioned above, with the increasing calcination temperature, the parent LDHs will gradually transform into MMO with spinel structure. Consequently, the calcination temperature had a non-negligible effect on the structural characteristic of MMO [140]. Theoretically, at low temperatures (about 200 °C), the calcined LDHs lose only weakly absorbed water and no oxide phases appears [49]. While as the temperature rose, the layered structure of LDHs would gradually disappear and form dense agglomerate [141]. Li et al. [142] researched the phase transition of MMO and interfaces of the catalysts calcined at different temperatures (400 °C, 500 °C, and 600 °C) over $Cu_1Co_2Fe_1$-LDHs precursors. A schematic illustration was displayed in Fig. 9a, the layered structure of LDHs collapsed after calcination, and the formed $Cu_1Co_2Fe_1O_x$-MMO phase was highly dependent on the calcination temperature. It had the most abundant phase interfaces (stage I) at 400 °C, while the catalysts are mainly composed of Co_3O4, Fe_3O_4 and CuO. As the temperature rose to 500 °C (stage II) and 600 °C (stage III), the partial oxides would interact to form spinel ($CoFe_2O_4$, $CuFe_2O_4$), thus the number of phase interfaces decreased with the phase transition. It was further confirmed by HR-TEM (Fig. 9b) images, where the microcrystal interacted and formed a multiphase interface at 500 °C. Notably, the formation of such enriched multiphase interfaces was shown to induce defect structures, thus favoring the formation of surface oxygen vacancies. As presented in ESR results (Fig. 9c), the $Cu_1Co_2Fe_1O_x$ with more diversified oxide phases exhibited a stronger oxygen vacancy signal (g = 2.004) compared to $Co_3Fe_1O_x$ and $Cu_3Fe_1O_x$. The oxygen vacancies are favored to adsorb free O_2 and generate activated oxygen, thereby contributing to the oxidation of VOCs molecules effectively. Moreover, the H_2-temperature programmed reduction (H_2-TPR) curves (Fig. 9d) also exhibited the superior low-temperature reducibility of $Cu_1Co_2Fe_1O_x$, which might attribute to the synergistic effect between multiple well-dispersed oxide phases. As a result, the $Cu_1Co_2Fe_1O_x$-MMO (calcined at 500 °C) performed the best in the catalytic oxidation of toluene (T_{90} = 246 °C, T_{90} represents the temperature where the removal rate is 90 %), which was much better than that of $Co_3Fe_1O_x$ (T_{90} = 318 °C) and $Cu_3Fe_1O_x$ (T_{90} = 315 °C).

Typically, the synthesis method determines the specific surface area, pore structure, non-stoichiometric oxygen, and reducibility of MMO to some extent, which are closely correlated with the catalytic performance [143]. As an example, the distinction of autocombustion (AC) and co-precipitation (CP) synthesis methods on the performance of $CoMnO_x$-MMO was investigated by Castano et al.[144]. By contrast, the MMO prepared by the AC method (Fig. 10a) exhibited a high porosity structure over the range of 1–5 μm and 100–300 nm, while the CP method (Fig. 10b) displayed smaller size pores (<100 nm). Moreover, the effect of two preparation methods on the reducibility of MMO was investigated by H_2-TPR (Fig. 10c), the hydrogen consumption of CPCoMn ($CoMnO_x$ prepared by CP method) at low temperatures (<400 °C) was significantly greater than that of ACCoMn ($CoMnO_x$ prepared by AC method), suggesting the superior low-temperature reducibility. We could figure out that the synthesis method had an indeed impact on the structure and properties of the MMO. In the AC method, the difference in the strength of the complexes with glycine (acts as a fuel) may inhibit the beneficial interaction of Co and Mn in the final oxides. In contrast, the CP method promotes the interaction between Co and Mn and forms solid solutions due to the long-term synthesis duration, which significantly improves the redox property and the oxygen mobility. Therefore, it exhibited better activity (T_{90} = 212 °C) than ACCoMn (T_{90} = 23 0 °C). Interestingly, the CoO_x-MMO prepared by the two methods showed similar catalytic activity (CoO_x-AC: T_{90} = 314 °C, CoO_x-CP: T_{90} = 312 °C), while the AC method favored the reducibil-

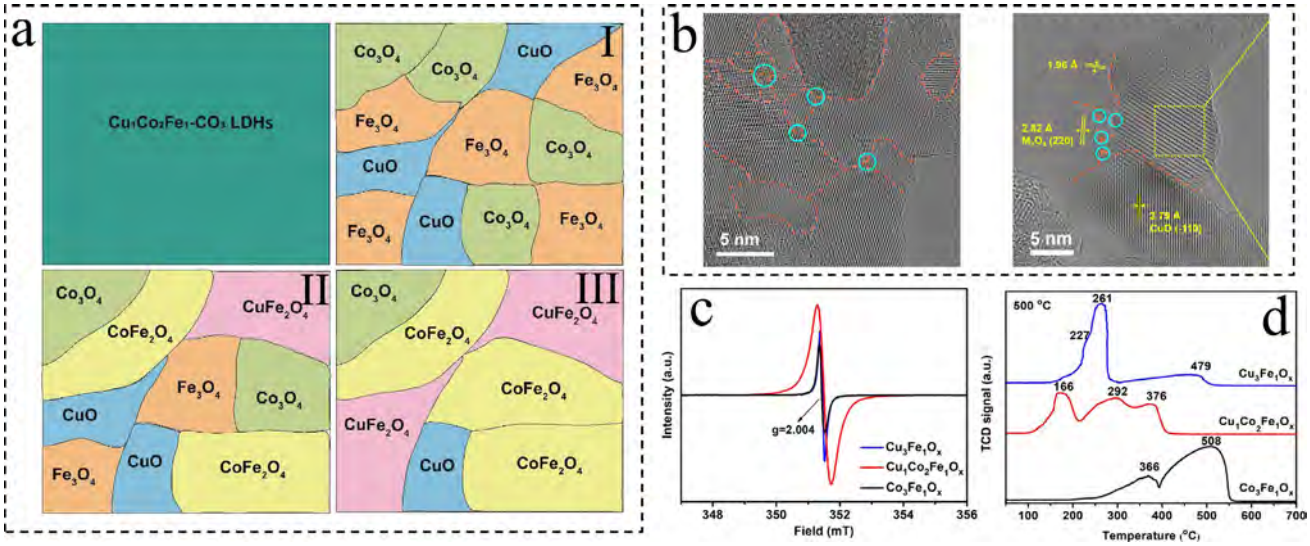

Fig. 9. (a) Schematic illustration of the phase transition of MMO and interfaces of the catalysts calcined at different temperatures (400 °C, 500 °C, and 600 °C) over $Cu_1Co_2Fe_1$-LDHs precursors. (b) HR-TEM images of $Cu_1Co_2Fe_1O_x$ calcined at 500 °C. (c) ESR spectra and (d) H_2-TPR profiles of $Co_3Fe_1O_x$, $Cu_1Co_2Fe_1O_x$, and $Cu_3Fe_1O_x$ catalysts calcined at 500 °C [142].

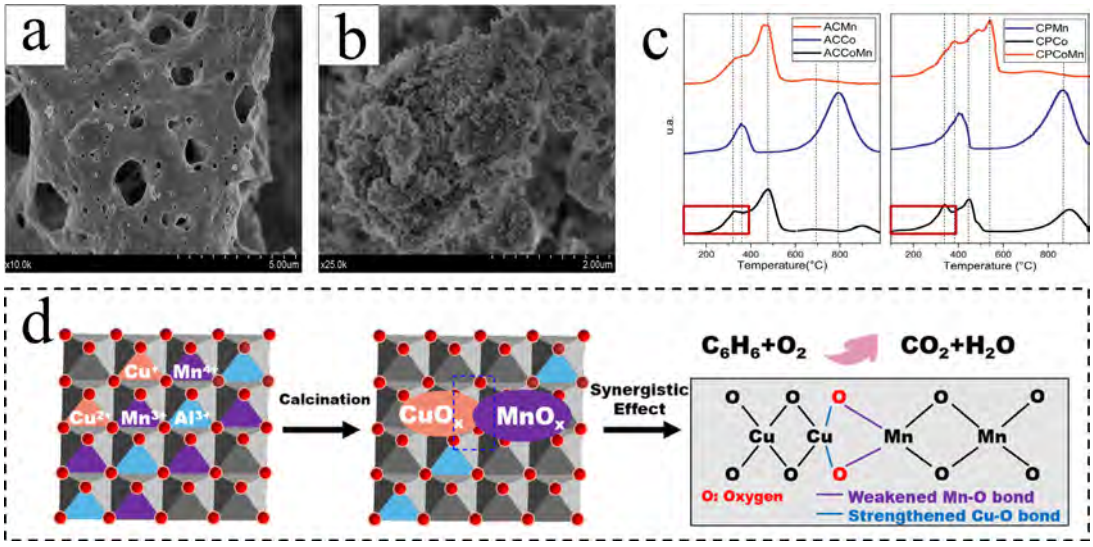

Fig. 10. (a) SEM images of (a) ACCoMn and (b) CPCoMn. (c) The H_2-TPR curves of the different MMO [144]. (d) Schematic of the thermal catalytic reaction mechanism of benzene over the $Cu_xMn_{2-x}Al$-O [145].

ity of MnO_x-MMO (Fig. 10c) and performed better (MnO_x-AC: T_{90} = 250 °C, MnO_x-CP: T_{90} = 280 °C). It seemed like the preparation methods had a distinct effect on different MMO catalysts. In another report, Zhang et al. [145] also investigated the different performance between MMO prepared by co-precipitation (Cu_x-$Mn_{2-x}Al$-O) and wet impregnation (CuO_x-MnO_x/Al_2O_3) methods. The $Cu_{0.5}Mn_{1.5}Al$-O performed best in the thermal catalytic oxidation of benzene (T_{90} = 193 °C). As shown in Fig. 10d, the enhanced activity was mainly contributed to the synergistic effect between MnO_x and CuO_x, where MnO_x accepted electrons from CuO_x, resulting in the weakening of the Mn-O bond and strengthening of the Cu-O bond, which promoted the replenishment of the adsorbed O_2 at reaction sites, thus facilitating the oxidation reactions of benzene.

Notably, the activity of $Cu_xMn_{2-x}Al$-O increased with the amount of Mn, it might partly attribute to the slightly higher specific surface area, larger pore volume, and smaller mean pore size than others, which favored active sites exposure and reactants diffusion. It implied that the metal ratios also had a significant effect on the performance of MMO. Recently, Deng et al. [146] investigated the impact of different Cr doping ratios on the catalytic performance of Co_3O_4 obtained from CoCr-LDHs precursors. It was found that the moderate incorporation of Cr significantly promoted the oxidation of chlorinated aromatic hydrocarbons, and inhibited the formation of polychlorinated by-products. The higher Cr content, the more significant the inhibition was. The addition of Cr was shown to produce more strong acid sites (mainly Lewis acid sites), which not only facilitated the adsorption/activation of chlorinated aromatics, but also reduced the deposition of Cl species on the surface of catalysts, thereby greatly improving the catalytic performance. Zhao et al. [147] also reported a promising catalytic activity (T_{90} = 173 °C for acetone, T_{90} = 175 °C for ethyl acetate) over Mn-doped $CoAlO_x$-MMO (Fig. 11a, $KMnO_4$ as precursor of Mn). Due to the sufficient reaction between $KMnO_4$ and Co^{2+}, the surface Mn cations were enriched in +3 and +4 valence, and rendered more surface Co^{3+}. The interactions between Co^{3+}/Co^{2+} and Mn^{4+}/Mn^{3+} could occur at the interface of MMO. Therefore, the appropriate amount of Mn was beneficial to improve the formation of active oxygen species and low-temperature reducibility. Moreover, Mn species had a crucial role in the thermal catalytic oxidation of VOCs. As shown in Fig. 11b, acetone was first adsorbed on the Co^{3+}-O-Mn^{x+} of the catalysts, where Co^{3+} acted as the main active sites. Then as the pollutants were oxidated to CO_2 by Co^{3+} and lattice oxygen, Co^{3+} was reduced to Co^{2+}, while the activated oxygen of MnO_x and free O_2 could re-oxidize the reduced Co^{2+} to Co^{3+}. It demonstrated a typical *Mars-van Krevelen* mechanism, which was generally applicable in the thermal catalytic oxidation of VOCs by MMO [148].

On the other hand, the structure of MMO is highly flexible regarding the contained cations. Divalent and trivalent cations generally occupy the A/B-sites, respectively. These cations can be substituted, mixed or converted, and the atoms of the corresponding valence randomly occupy their respective sites. The performance of MMO with different cations usually vary widely. Yang et al. [149] investigated the difference in the synergistic effect of transition metals with AlCo-LDHs and GaCo-LDHs as precursors. It was found that though the radius of Al^{3+} (0.50 Å) and Ga^{3+} (0.62 Å) were similar, the $GaCoO_x$-MMO exhibited better catalytic activity than $AlCoO_x$-MMO due to their higher surface active Co^{3+} content and reducibility. Wang et al. [150] further introduced Cu^{2+} at the A-site (Fig. 12a), it was presented in Fig. 12b that the CuCaGo exhibited better catalytic activity (T_{90} = 245 °C) for toluene compared with the prepared CoGa (T_{90} = 285 °C) and CuGa (T_{90} = 261 °C). The introduction of Cu at A-site was shown to promote low-temperature reducibility and the formation of adsorbed oxygen species by H_2-TPR (Fig. 12c) and O_2-TPD curves (Fig. 12d), which contributed to the oxidation reactions of toluene. Moreover, the intensified mechanism was proposed in Fig. 12f. Co species generally existed in both Co^{2+} and Co^{3+} forms, occupying the A/B-site, respectively. As the introduction of Cu^{2+} into the A-site, the electronegativity of Co^{2+} was indicated to decrease, which enabled Co^{2+} to gain more momentum for the conversion to Co^{3+}. Meanwhile, the lattice distortion caused by the difference in ionic radius of Cu^{2+} and Co^{2+} would make the enrichment of surface oxygen defects and adsorbed oxygen species. In addition, the B-site Ga^{3+} could also generate the pushing effect towards the B-site Co^{3+}, promoting Co^{3+} transfer to lower valence Co^{2+}. As a result, the conversion efficiency between Co^{2+} and Co^{3+} was improved, which greatly accelerated the redox cycle in the catalytic reaction.

4.3. Summary of typical LDHs-based thermocatalysts

LDHs-based materials are widely applied in the thermal catalytic oxidation of VOCs, and have shown promising performance.

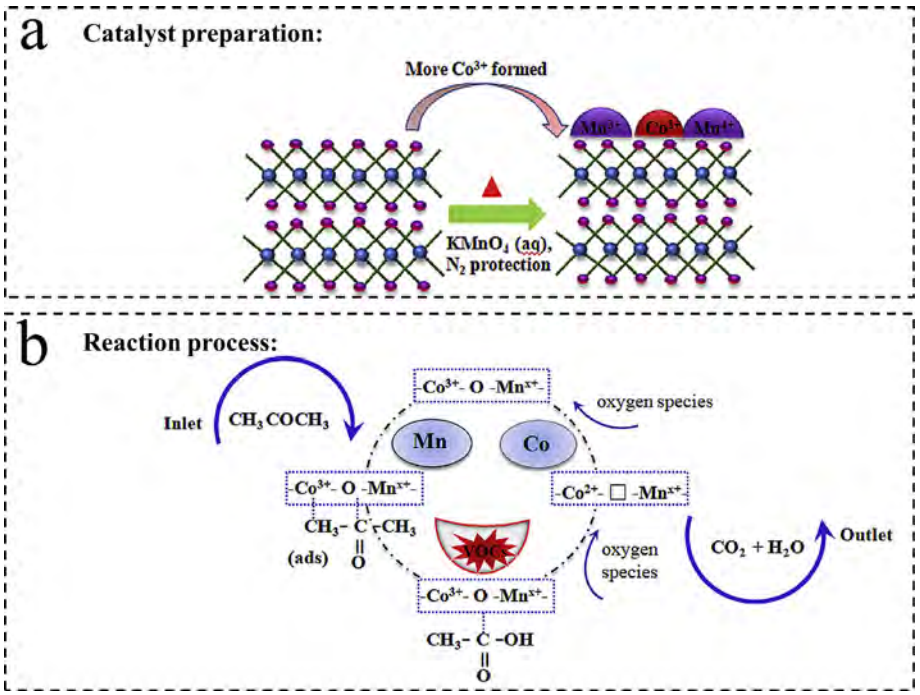

Fig. 11. (a) Preparation and (b) thermal catalytic oxidation pathways of Mn-doped $CoAlO_x$-MMO [147].

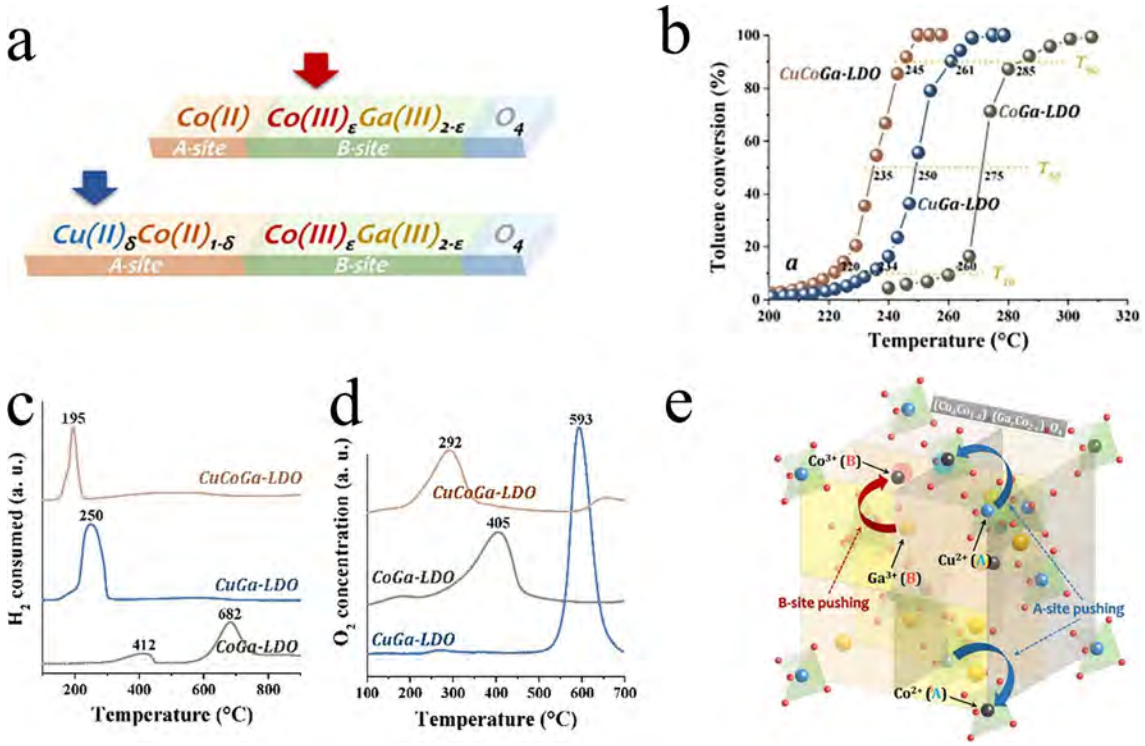

Fig. 12. (a) Binding sites for Cu (II), Co (II)/Co (III), Ga (III) in catalysts. (b) Toluene conversion rate, (c)H_2-TPR and (d) O_2-TPD curves of the prepared catalysts. (e) Mechanism diagram of the enhanced effect of CuCoGa catalysts [150].

On the one hand, LDHs can act as functional units to form multifunctional composites with other active centers (e.g., Pt, Au NPs). Since the abundant surface hydroxyl groups can adsorb/activate the VOCs molecules, LDHs composites exhibited surprising catalytic activity at low temperatures [114]. In addition, their unique layered structure is proven to facilitate the exposure and dispersion of the active centers [40]. It is also an attractive option to combine additional components (e.g., rGO, C_3N_4) with lamellar structure.

On the other hand, MMO based on the topological transformation of LDHs is the most popular form in the thermal catalytic oxidation of VOCs. To refine the design and preparation of more

optimal MMO catalysts, we discuss the influence of some factors: (i) calcination temperature: the calcination of LDHs precursors is favorable for the generation of defective structures, but the calcination temperature should be moderate to ensure the massive generation of mixed-metal multiphase interfaces, and the synergistic effect between multiple well-dispersed oxide phases has a vital role in the catalytic reactions; (ii) preparation method: the preparation method determines not only the morphological structure, but also the extent of beneficial interaction (synergistic effect) between different metal components in MMO; (iii) metal ratio: the appropriate metal ratio is helpful to reduce the deposition of toxic intermediates, and significantly improve the catalytic performance by promoting the oxygen mobility and reducibility; (iv) metal type: different metal cations types of MMOs tend to have significantly varying catalytic performance.

Table 3 is presented as a valuable reference to summarize the reported catalytic performance of different MMO and their intensified mechanisms. Notably, they are also supported on some substrates (e.g., iron mesh, Ni foam, cordierite) as monolithic catalysts with superior activity, which makes a great prospect for industrial applications [151–153].

5. The resistance of LDHs-based materials against complex gas components

The emissions of VOCs are inevitably accompanied by additional gas components such as sulfur-containing species, water vapor, CO, NO_x or other by-products, especially in coal-fired power plants [162,163], petrochemical industries [164], steel plants [165], and oil refinery [166]. Apart from the inherent features of LDHs-based materials, these additional gas components also have a non-negligible impact on the catalytic performance for VOCs abatement [167–169]. Therefore, to realize the industrialization of LDHs-based materials, not only the excellent activity and long-term stability should be pursued, but the resistance against complex gas components is also an important indicator to evaluate the performance of catalysts.

5.1. Sulfur-resistance of LDHs-based materials

In practical application, the presence of sulfur-containing species tends to put the catalyst at risk of poisoning. Due to sulfur/sulfate deposition on the active sites and pores, the sulfur-containing species such as SO_2 [170,171], H_2S [172,173], COS [174,175] and CS_2 [176,177] have been reported to have an irreversible effect on the catalytic performance. For LDHs-based materials, the exposed surface hydroxyl basic sites and high anion exchange capacity enable them to be effective adsorbents for acidic gases (e.g., H_2S [178], COS [179]). Othman et al. [178] had confirmed that the H_2S adsorbed into LDHs would be partially oxidized to sulfate and eventually deposited in the interlayer region. Therefore, LDHs-based materials may pose a risk of poisoning in sulfur-containing atmospheres. However, the effect of sulfur-containing species on VOCs abatement by LDHs was barely discussed in the existing research, even in studies of LDHs-based materials with the introduction of susceptible noble metals. It is necessary to make some discussion in this review.

In some scenarios, LDHs-based materials exhibit superior sulfur resistance in some reactions attributed to the porous structure and large specific surface area. For instance, Hong et al.[180] found only a slight decrease in Hg^0 adsorption of the CuS_x/LDHs after introducing 2000 ppm SO_2 to the simulated flue gas. Similar experimental results were reported by Yuan et al. over the S-modified LDHs [181]. Notably, the activity decreased more significantly in the pres-

Table 3
The summary of different MMO for thermal catalytic oxidation of VOCs and their intensified mechanisms.

Materials	Type	Synthesis methods	Experimental conditions	Catalytic activity (T_{90})	Intensified mechanisms	Ref.
$CoAlO_x$	Monometallic MMO	Homogeneous precipitation method, calcined at 400 °C	Catalyst: 100 mg; flow rate: 100 mL/min	100 ppm Benzene (T_{99}): 210 °C	Abundant surface adsorbed oxygen species, low-temperature reducibility, surface Lewis acid sites	[154]
Mn_3AlO_x	Monometallic MMO	Co-precipitation method, calcined at 550 °C	Catalyst: 200 mg; flow rate: 60 mL/min	258 ppm Acetone: 164 °C	Rich surface oxygen vacancy	[148]
Co_5AlO_x	Monometallic MMO	Co-precipitation method; calcined at 400 °C	Catalyst: 200 mg; flow rate: 110 mL/min	1000 ppm Acetone: 222 °C	Low-temperature reducibility, abundant surface Co^{3+}species, favorable crystallinity and porous structure	[155]
$Cu_{0.5}Co_{2.5}AlO_x$	Bimetallic MMO	*In situ* crystallization on a pure aluminium substrate; calcined at 400 °C	Catalyst: 100 mg; flow rate: 100 mL/min	1000 ppm Benzene: 290 °C	Larger surface area, smaller pore size, promoted adsorption of oxygen, better inter-dispersion of the oxide phase	[156]
Co_2NiAlO_x	Bimetallic MMO	*In situ* crystallization on a pure aluminium substrate; calcined at 400 °C	Catalyst: 100 mg; flow rate: 100 mL/min	100 ppm Toluene: 227 °C	Larger surface area, abundant surface Co^{3+}, and adsorbed oxygen species	[157]
Co_3CrO_x	Bimetallic MMO	Co-precipitation and hydrothermal methods, calcined at 400 °C	Catalyst: 100 mg; flow rate: 100 mL/min	1000 ppm 1,2-dichlorobenzene: 288 °C	Smaller crystallite size, promoted lattice oxygen mobility and acidic properties, uniform particle size distribution	[146]
$Co_{4.75}Cu_{0.25}AlO_x$	Bimetallic MMO	Co-precipitation method, calcined at 600 °C	Catalyst: 100 mg; flow rate: 60 mL/min	100 ppm Benzene: 306 °C	Improved reducibility of Co^{3+} active species	[158]
$CeMnAlO_x$	Bimetallic MMO	Co-precipitation method, calcined at 400 °C	Catalyst: 100 mg; flow rate: 100 mL/min	100 ppm Benzene: 210 °C	Low-temperature reducibility, abundant surface lattice oxygen species, promoted electron transfer	[159]
$CoMn_2AlO_x$	Bimetallic MMO	*In situ* crystallization on pure aluminum substrate, calcined at 550 °C	Catalyst: 100 mg; flow rate: 100 mL/min	100 ppm Benzene: 208 °C	Great low-temperature reducibility, abundant surface Co^{3+}, Mn^{4+} and adsorption oxygen species	[160]
$Cu_2Co_2MnAlO_x$	Trimetallic MMO	Hydrothermal method, calcined at 500 °C	Catalyst: 500 mg; flow rate: 200 mL/min	5 g/m^3 Toluene: 235 °C	Enhanced reducibility and oxygen mobility, promoted the formation of oxygen vacancy	[161]
$Cu_1Co_2Fe_1O_x$	Trimetallic MMO	Co-precipitation method, calcined at 500 °C	Catalyst: 100 mg; flow rate: 100 mL/min	800 ppm Toluene: 238 °C	Abundant oxygen vacancy, formation of multi-face interfaces	[142]

ence of O_2. It can be explained by the fact that oxygen accelerates the formation of sulfate to some extent [182]. In addition, the LDHs derived MMO also showed excellent sulfur resistance in NH_3-selective catalytic reduction (NH_3-SCR) reactions [183,184]. As an example, the $Cu_1Mn_{0.5}Ti_{0.5}O_x$-MMO showed only a slight decrease in NO_x conversion after the introduction of 100 ppm SO_2 for 12 h [185]. Notably, after the sulfate species formed and deposited on the surface, the specific surface area of $Cu_1Mn_{0.5}Ti_{0.5}O_x$-MMO decreased to a certain extent (from 102.1 m^2/g to 69.3 m^2/g), which might be the possible reason for the decreased activity. Beside, Jayaprakash et al. [186] reported that the MMO could oxidize some deposited metal sulfates to other sulfur oxides, which released the active sites. Therefore, although the inevitable formation of surface sulfate species leads to a slight decrease in catalytic activity, LDHs-based materials are expected to have excellent sulfur resistance.

5.2. Water-resistance of LDHs-based materials

It is reported that water vapor will compete for the active sites and continue to accumulate, which may eventually lead to the deactivation of catalysts [187,188]. Generally, the inhibitory effect of water vapor was more evident at relatively low temperatures during the thermal catalytic oxidation of VOCs by LDHs-derived MMO. As an example, the benzene conversion decreased from 97.2 % to 88.8 % over the Co_xNiAlO-MMO after introducing 3.5 vol% H_2O at 240 °C, while the negative effect was negligible at 260 °C [157]. Mo et al.[160] also found that the inhibitory effect of water vapor was reduced with the increasing reaction temperature (benzene conversion decreased from 57.8 % to 41.5 % at 190 °C, while unchanged at 230 °C). The reasons behind this phenomenon might be the reaction temperature exceeded the H_2O desorption temperature in the high-temperature environment [148]. Besides, O_2 molecules were more likely to be activated with the increasing temperature, where the adsorption of O_2 might be stronger than H_2O [189]. Moreover, the MMO showed excellent stability in thermal catalytic oxidation of VOCs under water-containing atmosphere. For example, in a 14 h benzene stream (500 ppm) with 1.5 vol% H_2O, the catalytic activity of the $Cu_{0.5}Co_{2.5}Al$-MMO only slightly decreased from 93.8 % to 91.7 % [156], and Mo et al. also reported the stable removal efficiency of MMO for benzene (from 99 % to 97 %) within 12 h after introducing 3.6 vol% H_2O [154]. Notably, the occupation of the active sites by water vapor is reversible. After removing the water vapor, their activity was subsequently recovered. Overall, the MMO catalysts can withstand the inhibitory effect of water vapor and maintain their superior catalytic activity to a certain extent.

On the other hand, the introduction of water vapor can also induce a facilitating effect in photocatalytic reaction·H_2O molecules have been known as an essential contributor to ·OH radicals in the photocatalytic process [190], and LDHs possess excellent H_2O absorption properties and dense surface hydroxyl groups [73,74,191]. Thus, the conversion of surface H_2O molecules and hydroxyl groups to ·OH radicals result in the unique water vapor resistance of LDHs [192,193]. As an example, Dong et al.[79] reported a unique H_2O-independent activity over TiO_2/MgAl-LDHs composites in photocatalytic oxidation of toluene. The results in Fig. 13a indicated that the catalytic activity ranged from 73.2 % to 84.3 % as the relative humidity (RH) increased from 0 to 90 %. The relationship between the generation of ·OH radicals and the H_2O adsorption behavior were investigated by the in-situ Fourier transform infrared (FT-IR) spectroscopy (Fig. 13b, c). A significant positive peak at 3695 cm^{-1} could be observed in Fig. 13b,

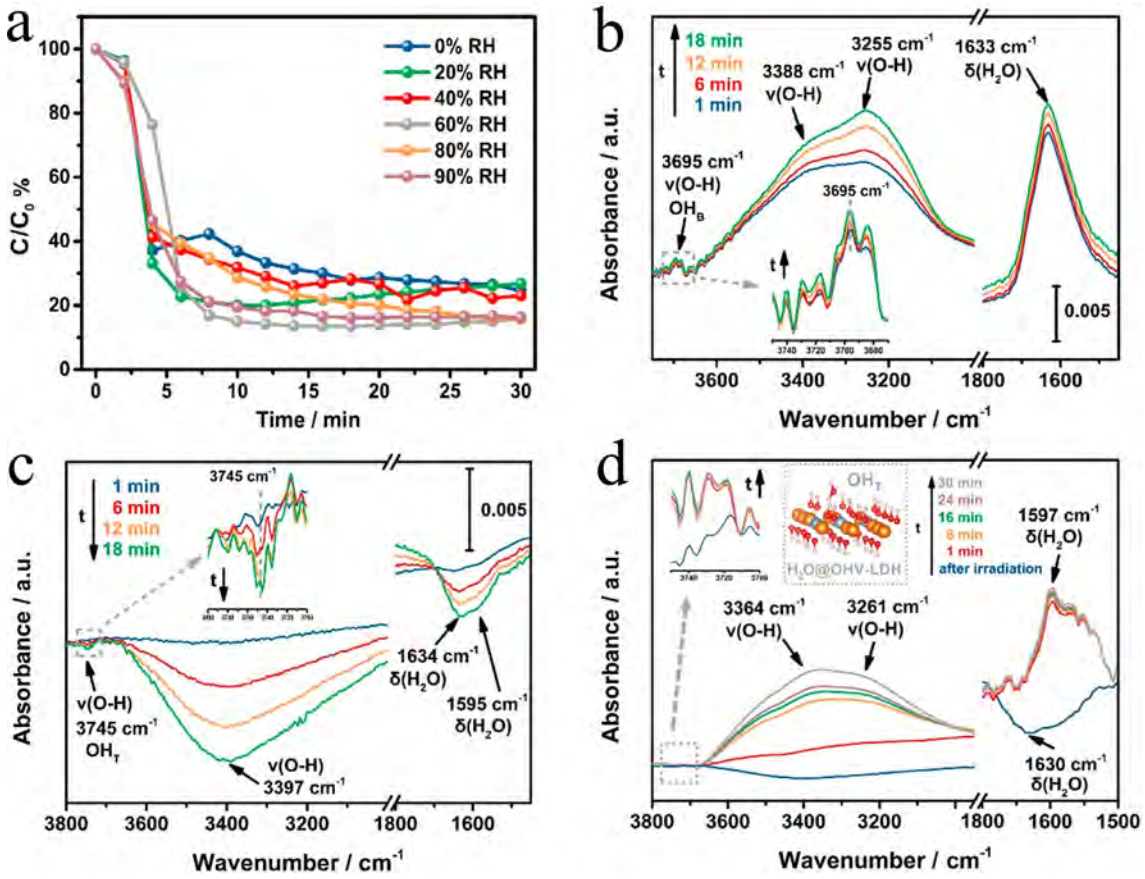

Fig. 13. (a) Photocatalytic activity of TiO_2/MgAl-LDHs under different relative humidity. In-situ FT-IR spectra of (b) the adsorption process of H_2O and (c) the characteristic group changes under light irradiation. (d) The H_2O adsorption process after irradiation for TiO_2/MgAl-LDHs [79].

suggesting that the density of bridged hydroxyl groups (OH_B) increased with the adsorption of H_2O. While under the light irradiation (Fig. 13c), two negative peaks (3700–3000 cm^{-1}, 1634 and 1595 cm^{-1}) indicated the loss of abundant surface-bound H_2O molecules, and the peak intensity of the terminal hydroxyl group (3745 cm^{-1}) also showed a tendency to decrease. Therefore, there was a tendency for the charge carriers to transfer from LDHs to TiO_2, where the isolated surface hydroxyl groups on LDHs lost electrons and became free, generating ·OH radicals at the edge of LDHs. Interestingly, as shown in Fig. 13d, after turning off the light and introducing the water vapor, the H_2O molecules tended to adsorb on the hydroxyl-deficient surface and compensated for the depletion of hydroxyl groups on LDHs surface, which restored their surface structure to original form. Similarly, Wang et al.[40] also reported that the moderate H_2O could compensate for the dynamic loss of the surface hydroxyl groups of LDHs. As a result, toluene could be efficiently oxidized at a wide humidity range. Nevertheless, under high RH conditions, excess H_2O may compete with VOCs molecules for adsorption sites, and even block small mesopores that act as mass transfer channels, thus reducing the catalytic activity (e.g., the activity at 90 % RH is lower than that at 60 % RH in Fig. 13a) [194]. Hence, it is reasonable to assume that LDHs-based materials also exhibit excellent water resistance in photocatalytic oxidation of VOCs. When the contribution of H_2O and surface hydroxyl groups to ·OH radicals outweigh the inhibition of H_2O, it shows that water vapor promotes the photocatalytic reaction overall.

5.3. The resistance of LDHs-based materials to NO_x and CO

Since LDHs-based materials are also effective SCR catalysts for NO_x elimination [195,196], VOCs molecules will inevitably compete with NO_x for active sites. As an example, Mrad et al. [197] found that there was a slight decrease in the conversion of propylene after introducing NO over the $Cu_xMg_{4-x}AlFeO_x$-MMO, while the conversion curve of NO increased initially and then decreased upon reaching the temperature point for complete oxidation of propylene. It was consistent with the research of Yuan et al. [198]. In contrast, with the introduction of CO, an increase in catalytic activity towards toluene could be observed on $Mg_6Al_{2-x}Ce_xO_x$-MMO [199]. It could attribute to the exothermicity of the CO oxidation reaction. The complete oxidation temperature of CO was lower than toluene, which enabled CO to be oxidized firstly and released heat, which caused an increased local temperature of the metal active sites. Hence, the catalytic activity of toluene was improved. Similar results had been reported by Genty et al. [200]. Notably, the activity on CeO_2 for toluene was slightly inhibited after introducing CO. It suggested that the competition between CO and toluene for the active sites also existed on the surface of catalysts. Although there are few studies on this topic, LDHs-based materials still show great potential for practical applications.

6. Other applications of LDHs-based materials in VOCs abatement

In addition to the photo/thermal catalytic oxidation of VOCs, LDHs-based materials are applied in other fields, such as adsorption, sensing, and vapor reforming of VOCs. It will be introduced in detail below.

6.1. LDHs-based materials as adsorbents

The unique layered structure and tunable structural units (e.g., metal cations or basic sites) of LDHs enable them to possess abundant adsorption sites for various contaminants [42]. Thus, LDHs-based materials can also serve as effective adsorbents for VOCs. As reported by Li et al.[201], the zeolite@LDHs composites showed a superior toluene adsorption capacity with a maximum breakthrough time of 77 min. Notably, the introduction of LDHs had greatly improved the poor water resistance of traditional zeolites, the breakthrough time was increased from 6.4-10.8 min to 20.1–27.5 min under wet conditions. Moreover, it was demonstrated that the inclusion of LDHs as adsorbents showed a significant inhibitory effect on VOCs emissions from bituminous materials [202,203]. Cui et al.[202] found that the 4 wt% MgAl-LDHs contributed the most to the reduction of VOCs emission rate and volatilization (Fig. 14a). The residual volatile speed was reduced to 0.4–0.6, which implied that the VOCs emission could be reduced by 40 %−60 %. Interestingly, the LDHs had a more significant effect on the volatile speed of small molecules, and the smaller the molecule, the more rapidly the volatile speed decreased.

6.2. LDHs-based materials as sensors

In addition to end-of-pipe treatment technologies, the presence of some hazardous VOCs (e.g., acetone, toluene) in the atmosphere also imposes higher demands on air quality detection. Recently, LDHs-based materials have been applied to fabricate highly sensitive, selective, and stable VOCs sensors. In general, the VOCs sensing processes refer to the chemical reactions that occur on the surface of materials. When gaseous O_2 in the air is adsorbed on the surface, the reduction reaction occurs to generate active oxygen species, and further participate in the oxidation process of VOCs molecules by the same mechanism as the thermal catalytic oxidation [205,206]. LDHs-based materials have exhibited great potential for detecting trace VOCs due to the diversity in chemical composition and structural characteristics.

Four LDHs (ZnAl-Cl, ZnFe-Cl, ZnAl-NO_3, and MgAl-NO_3) were synthesized as sensing elements by Vigna et al.[204] (Fig. 14b). It was found that the LDHs with high porosity not only provided multiple diffusion channels allowing rapid diffusion of the gas, but increased the numbers of active sites on the surface and inside the bulk. As a result, all LDHs-based sensors showed excellent VOCs-sensitive properties, and were capable of reversible and selective detection of acetone with sensing response values up to 6 % at room temperature. Moreover, Nie et al.[141] suggested that the gas sensors from LDHs derived MMO also achieve an outstanding VOCs sensing performance due to the formation of heterojunction. The response of prepared Ni_xGaO-MMO to toluene was 10.54–5 ppm at 200 °C, and it showed a trend of increasing and then dropping with increasing temperature between 175 °C and 250 °C. Typically, the operating temperature tends to affect the surface oxygen species, charge carrier content, desorption and adsorption rates of the materials, which have a profound impact on gas sensing performance. At relatively low temperatures, increasing the temperature would result in a higher adsorption and desorption rate, however, once the temperature attained certain high values, the consequent high desorption rate was not favorable for the gas sensing response. Besides, the Ni_xGaO-MMO also showed excellent water resistance and stability. Currently, researchers aim at modulating the response by changing specific chemical structures based on various LDHs, and fabricating low-cost materials for low-temperature detection of more specific gases at relatively low concentrations.

6.3. LDHs-based materials for steam reforming

Catalytic steam reforming has received much attention from researchers for its ability to convert hazardous organic compounds into valuable products at low temperatures [207]. LDHs-based

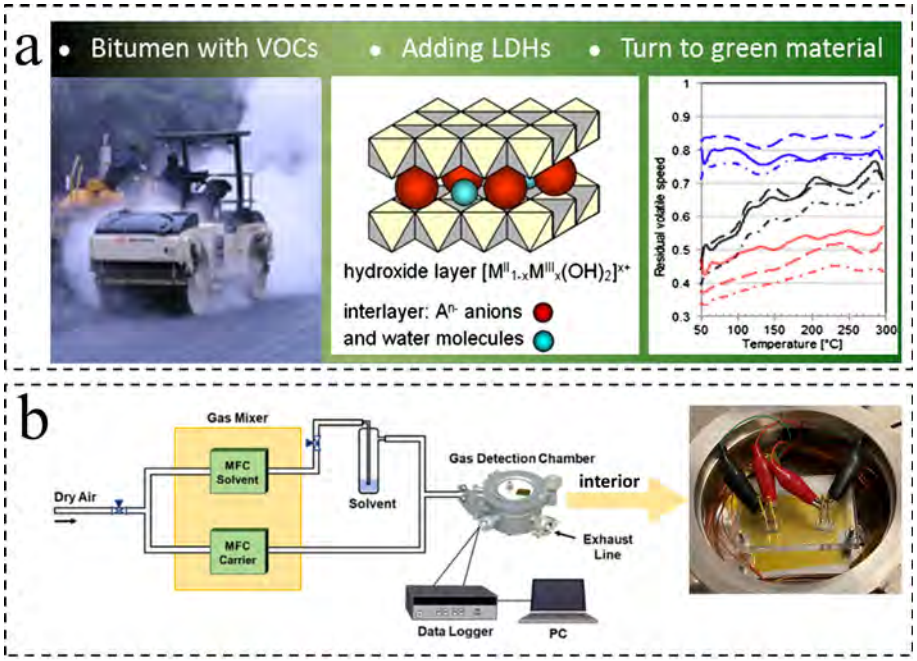

Fig. 14. (a) Using MgAl-LDHs to reduce the VOCs from bituminous materials [202]. (b) Scheme of the experimental sensing of LDHs [204].

materials also have good prospects in the steam reforming of toluene. For example, Mitran et al.[208] evaluated the catalytic activity of Mo catalysts derived from LDHs, it was found that the toluene conversion and hydrogen production were positively related to temperature. At 500 °C, the $Mo_{4.5}$MgAl-MMO exhibited the highest toluene conversion of 64.3 % and hydrogen amount of 60.7 %. The MgAlV-MMO catalysts showed the same trend [209]. Most recently, Kawi et al.[186] achieved 96 % toluene conversion over LDHs derived CeO_2-NiO-MgO-Al_2O_3 (Ce-NMA) catalysts at 750 °C. There was less carbon deposition after the introduction of Ce in the reforming reaction. It was probably due to the amorphous nature of the carbon in Ce-NMA-MMO catalysts, which was easier to remove and burn from the surface. The Ce-NMA-MMO also exhibited excellent sulfur resistance and stability.

Furthermore, the use of LDHs-based materials in other environmental applications has increased substantially, including wastewater treatment [210,211], water splitting [212,213], CO_2 reduction [214–216]. It is expected that LDHs-based catalysts will become one of the most promising candidates in various important areas.

7. Conclusions and prospects

As demonstrated in this review, LDHs-based materials represent one of the most promising and effective catalysts for VOCs abatement. By virtue of the fine tunability (chemical composition, electronic structure, and morphology) and the versatility of LDHs, they can be formed into various composites with other functional units through a variety of optimization strategies (e.g., support, assembly, modification, and topotactic transformation). In addition, their superior properties, including low cost, facile preparation, stability, unique layered structure, and abundant surface hydroxyl groups, provide ample potential for practical applications. This paper provides a systematic overview of various LDHs-based catalysts for VOCs abatement (mainly in the field of photo/thermal catalytic oxidation), especially the intensified mechanisms for optimizing their catalytic performance are highlighted. Moreover, the effect of different gas components (e.g., SO_2, H_2S, H_2O, CO, NO_x) on the catalytic performance of LDHs-based materials is examined. Currently, although the applications of LDHs-based materials for VOCs abatement are emerging at a growing rate, there are still several challenges to overcome:

(i) Since the property and function of LDHs depend primarily on their unique structure and special synthesis method, their high quality and phase purity must be ensured, which impose more demands during the preparation process of LDHs [46]. Besides, the synthesis of LDHs-based materials with desirable functions, such as high crystallinity and dispersion, sufficient exposed active sites (e.g., shell-core structured LDHs), precisely controlled particle size and morphology (e.g., supported LDHs), is usually too complicated for practical application. Therefore, in the future, the critical goal is to further optimize the preparation process, and replace the noble metals with cheaper and more abundant materials to shrink the cost. Additionally, it is necessary to make the preparation process more environmentally friendly and improve the convenience of recovery and recycling, enabling the large-scale application of LDHs.

(ii) For LDHs derived MMO, the formation and conversion of the multiphase interfaces during the topological transformation of LDHs precursors is not clarified yet. It is necessary to apply advanced physicochemical techniques to in-situ monitor the topological transformation of LDHs precursors to MMO, so as to understand the effects of structural conversion and the interactions between various oxide phases on active species.

(iii) Various LDHs-based catalysts with excellent activity have been engineered and applied in the catalytic reaction of VOCs. However, it is always a challenge to identify the catalytic active centers in LDHs-based composites, which will limit the targeted design and controlled synthesis of composites with the desired active sites. Moreover, the catalytic mechanisms in photo/thermal catalytic oxidation of VOCs have not been fully interpreted. Therefore, the exploration of new characterization techniques and approaches to investigate the nature of the active centers, the synergistic effect between each active components, and the consequent catalytic mechanism is significant.

(iv) As efficient photocatalysts, LDHs-based materials remain to be advanced. As the most popular LDHs-based photocatalysts, supported LDHs can further explore the structure with a large surface

area, such as multilayer LDHs, so that strong adsorption on the target VOCs can be achieved. In addition, the development of noble metal alloys with optimized atomic ratios (e.g., AuPt, AuCu, and AuNi alloys) is seen as one of the strategies to improve the catalytic performance of the supported LDHs [217,218]. Exploiting the LSPR effect of noble metals to develop visible light or even near infrared light-driven photocatalytic reactions also has profound implications for the utilization of sunlight. On the other hand, as for thermal catalytic oxidation, the extended trimetallic or tetrametallic multiphase MMO derived from LDHs have shown promising catalytic performance and stability [161,219,220]. It deserves deeper study by researchers for further improvement of functionality.

(v) In this review, we have discussed the resistance of LDHs-based materials against complex gas components (SO_2, H_2O, NO_x, CO, etc.). However, it is insufficient to provide an overall evaluation of the resistance of LDHs-based materials, more studies are required to examine the effect of other gas components (e.g., CO_2, CO, NH_3). More importantly, the synergistic influence of different gas components (e.g., H_2O and SO_2) may result in a further decrease of the catalytic performance [185], which deserves more attention from the researchers in the upcoming work. Furthermore, in practical applications, the properties of LDHs-based catalysts in terms of deactivation (e.g., coking, poisoning, and sintering) and regeneration needs to be further investigated. Their long-term stability, reversibility, and durability under specific atmospheres should be also systematically researched.

LDHs-based materials have shown great potential as novel catalysts for VOCs abatement. In further studies, the innovation of synthesis strategies and the compositing of LDHs with other functional materials will create new possibilities. We believe that the application of LDHs-based materials for VOCs abatement will continuously and rapidly expand in the foreseeable future.

Declaration of Competing Interest

The authors declare that they have no known competing financial interests or personal relationships that could have appeared to influence the work reported in this paper.

Acknowledgements

This work was supported by the Key Research and Development Program of Hunan Province in China (2018SK2032, 2018SK2033) and the National Key Research and Development Program of China (2016YFC0204100).

References

[1] X.-L. Cao, M. Sparling, R. Dabeka, Food Addit. Contam. 33 (2016) 373–382.
[2] S. Ojala S. Pitkäaho T. Laitinen N. Niskala Koivikko R. Brahmi J. Gaálová L. Matejova A. Kucherov S. Päivärinta C. Hirschmann T. Nevanperä M. Riihimäki M. Pirilä R.L. Keiski Top. Catal. 54 (2011) 1224.
[3] W.B. Li, J.X. Wang, H. Gong, Catal. Today 148 (2009) 81–87.
[4] Y. Liu, J. Deng, S. Xie, Z. Wang, H. Dai, Chin. J. Catal. 37 (2016) 1193–1205.
[5] B. Ozturk, D. Yilmaz, Process Saf. Environ. Prot. 84 (2006) 391–398.
[6] M. Ousmane, L.F. Liotta, G.D. Carlo, G. Pantaleo, A.M. Venezia, G. Deganello, L. Retailleau, A. Boreave, A. Giroir-Fendler, Appl. Catal. B-Environ. 101 (2011) 629–637.
[7] M.S. Kamal, S.A. Razzak, M.M. Hossain, Atmos. Environ. 140 (2016) 117–134.
[8] A.G. Carlton, C. Wiedinmyer, J.H. Kroll, Atmos. Chem. Phys. 9 (2009) 4987–5005.
[9] M. Amann, M. Lutz, J. Hazard. Mater. 78 (2000) 41–62.
[10] J. Finlayson-Pitts Barbara, N. Pitts James, Science 276 (1997) 1045–1051.
[11] L.F. Liotta, Appl. Catal. B-Environ. 100 (2010) 403–412.
[12] S. Scirè, L.F. Liotta, Appl. Catal. B-Environ. 125 (2012) 222–246.
[13] J. Zhang, J. Xiao, X. Chen, X. Liang, L. Fan, D. Ye, J. Environ. Sci. 69 (2018) 155–165.
[14] K. Qiu, L. Yang, J. Lin, P. Wang, Y. Yang, D. Ye, L. Wang, Atmos. Environ. 86 (2014) 102–112.
[15] T. Chang, Y. Wang, Y. Wang, Z. Zhao, Z. Shen, Y. Huang, S.K.P. Veerapandian, N. De Geyter, C. Wang, Q. Chen, R. Morent, Sci. Total Environ. 828 (2022) 154290.
[16] X. Wu, R. Han, Q. Liu, Y. Su, S. Lu, L. Yang, C. Song, N. Ji, D. Ma, X. Lu, Catal. Sci. Technol. 11 (2021) 5374–5387.
[17] A.H. Mamaghani, F. Haghighat, C.-S. Lee, Appl. Catal. B-Environ. 203 (2017) 247–269.
[18] Z. Shayegan, C.-S. Lee, F. Haghighat, Chem. Eng. J. 334 (2018) 2408–2439.
[19] C. He, J. Cheng, X. Zhang, M. Douthwaite, S. Pattisson, Z. Hao, Chem. Rev. 119 (2019) 4471–4568.
[20] Z. Cheng, W. Qi, C.H. Pang, T. Thomas, T. Wu, S. Liu, M. Yang, Adv. Funct. Mater. 31 (2021) 2100553.
[21] K. Everaert, J. Baeyens, J. Hazard. Mater. 109 (2004) 113–139.
[22] B. Song, C. Li, X. Du, S. Li, Y. Zhang, Y. Lyu, Q. Zhou, Fuel 306 (2021) 121654.
[23] X. Du, C. Li, L. Zhao, J. Zhang, L. Gao, J. Sheng, Y. Yi, J. Chen, G. Zeng, Appl. Catal. B-Environ. 232 (2018) 37–48.
[24] S.S.T. Bastos, J.J.M. Órfão, M.M.A. Freitas, M.F.R. Pereira, J.L. Figueiredo, Appl. Catal. B-Environ. 93 (2009) 30–37.
[25] D. Yu, Y. Liu, Z. Wu, Catal. Commun. 11 (2010) 788–791.
[26] W. Tang, X. Wu, S. Li, W. Li, Y. Chen, Catal. Commun. 56 (2014) 134–138.
[27] Y. Shu, J. Ji, Y. Xu, J. Deng, H. Huang, M. He, D.Y.C. Leung, M. Wu, S. Liu, S. Liu, G. Liu, R. Xie, Q. Feng, Y. Zhan, R. Fang, X. Ye, Appl. Catal. B-Environ. 220 (2018) 78–87.
[28] Y. Zheng, Q. Liu, C. Shan, Y. Su, K. Fu, S. Lu, R. Han, C. Song, N. Ji, D. Ma, Environ. Sci. Technol. 55 (2021) 5403–5411.
[29] J. Chen, X. Chen, X. Chen, W. Xu, Z. Xu, H. Jia, J. Chen, Appl. Catal. B-Environ. 224 (2018) 825–835.
[30] C.G. Silva, Y. Bouizi, V. Fornés, H. García, J. Am. Chem. Soc. 131 (2009) 13833–13839.
[31] X. Li, J. Yu, M. Jaroniec, Chem. Soc. Rev. 45 (2016) 2603–2636.
[32] Y. Wu, H. Wang, Y. Sun, T. Xiao, W. Tu, X. Yuan, G. Zeng, S. Li, J.W. Chew, Appl. Catal. B-Environ. 227 (2018) 530–540.
[33] F.-D. Zhang, C.-G. Lin, S.-J. Diao, H.N. Miras, Y.-F. Song, Inorg. Chem. Front. 8 (2021) 1324–1333.
[34] B. Li, J. He, D.G. Evans, X. Duan, Appl. Clay Sci. 27 (2004) 199–207.
[35] R. Liang, R. Tian, L. Ma, L. Zhang, Y. Hu, J. Wang, M. Wei, D. Yan, D.G. Evans, X. Duan, Adv. Funct. Mater. 24 (2014) 3144–3151.
[36] Y. Zhao, X. Jia, G.I.N. Waterhouse, L.-Z. Wu, C.-H. Tung, D. O'Hare, T. Zhang, Adv. Energy Mater. 6 (2016) 1501974.
[37] M. Zubair, M. Daud, G. McKay, F. Shehzad, M.A. Al-Harthi, Appl. Clay Sci. 143 (2017) 279–292.
[38] C. Taviot-Guého, V. Prévot, C. Forano, G. Renaudin, C. Mousty, F. Leroux, Adv. Funct. Mater. 28 (2018) 1703868.
[39] Y.K. Jo, J.M. Lee, S. Son, S.-J. Hwang, J. Photochem. Photobiol., C 40 (2019) 150–190.
[40] Y. Wang, C. Jiang, Y. Le, B. Cheng, J. Yu, Chem. Eng. J. 365 (2019) 378–388.
[41] J.C.A.A. Roelofs, D.J. Lensveld, A.J. van Dillen, K.P. de Jong, J. Catal. 203 (2001) 184–191.
[42] C. Li, M. Wei, D.G. Evans, X. Duan, Small 10 (2014) 4469–4486.
[43] G. Zhang, X. Zhang, Y. Meng, G. Pan, Z. Ni, S. Xia, Chem. Eng. J. 392 (2020) 123684.
[44] X. Guo, F. Zhang, D.G. Evans, X. Duan, Chem. Commun. 46 (2010) 5197–5210.
[45] J. Feng, Y. He, Y. Liu, Y. Du, D. Li, Chem. Soc. Rev. 44 (2015) 5291–5319.
[46] L. Mohapatra, K. Parida, J. Mater. Chem. A 4 (2016) 10744–10766.
[47] H. Yin, Z. Tang, Chem. Soc. Rev. 45 (2016) 4873–4891.
[48] T. Li, H.N. Miras, Y.-F. Song, Catalysts 7 (2017).
[49] H. Ye, S. Liu, D. Yu, X. Zhou, L. Qin, C. Lai, F. Qin, M. Zhang, W. Chen, W. Chen, L. Xiang, Coord. Chem. Rev. 450 (2022) 214253.
[50] S. Li, D. Wang, X. Wu, Y. Chen, Chin. J. Catal. 41 (2020) 550–560.
[51] M.V. Bukhtiyarova, J. Solid State Chem. 269 (2019) 494–506.
[52] G. Fan, F. Li, D.G. Evans, X. Duan, Chem. Soc. Rev. 43 (2014) 7040–7066.
[53] S. Xia, L. Zhang, X. Zhou, G. Pan, Z. Ni, Appl. Clay Sci. 114 (2015) 577–585.
[54] F. Cavani, F. Trifirò, A. Vaccari, Catal. Today 11 (1991) 173–301.
[55] L. Obalová, K. Karásková, K. Jirátová, F. Kovanda, Appl. Catal. B-Environ. 90 (2009) 132–140.
[56] A.W. Musumeci, Z.P. Xu, S.V. Smith, R.F. Minchin, D.J. Martin, J. Nanopart. Res. 12 (2010) 111–120.
[57] K. Nejati, H. Keypour, P.D.K. Nezhad, K. Asadpour-zeynali, Z. Rezvani, Mol. Cryst. Liq. Cryst. 608 (2015) 177–189.
[58] T. Vulic, A. Reitzmann, J. Ranogajec, R. Marinkovic-Neducin, J. Therm. Anal. Calorim. 110 (2012) 227–233.
[59] T.K.N. Nguyen, Y. Matsui, N. Shirahata, N. Dumait, S. Cordier, F. Grasset, N. Ohashi, T. Uchikoshi, Appl. Clay Sci. 196 (2020) 105765.
[60] Y. Hou, S. Qiu, Y. Hu, C.K. Kundu, Z. Gui, W. Hu, A.C.S. Appl, Mater. Inter. 10 (2018) 18359–18371.
[61] K. Nejati, A.R. Akbari, S. Davari, K. Asadpour-Zeynali, Z. Rezvani, New J. Chem. 42 (2018) 2889–2895.
[62] A. Edenharter, P. Feicht, B. Diar-Bakerly, G. Beyer, J. Breu, Polymer 91 (2016) 41–49.
[63] S. Omwoma, W. Chen, R. Tsunashima, Y.-F. Song, Coord. Chem. Rev. 258–259 (2014) 58–71.
[64] R. Guo, L.-C. Nengzi, Y. Chen, Y. Li, X. Zhang, X. Cheng, Chem. Eng. J. 398 (2020) 125676.
[65] M.-Q. Zhao, Q. Zhang, W. Zhang, J.-Q. Huang, Y. Zhang, D.S. Su, F. Wei, J. Am. Chem. Soc. 132 (2010) 14739–14741.
[66] J. Cai, J. Huang, Y. Lai, J. Mater. Chem. A 5 (2017) 16412–16421.

[67] I. Paramasivam, H. Jha, N. Liu, P. Schmuki, Small 8 (2012) 3073–3103.
[68] J. Liu, G. Zhang, Phys. Chem. Chem. Phys. 16 (2014) 8178–8192.
[69] G. Liu, J. Ji, P. Hu, S. Lin, H. Huang, Appl. Surf. Sci. 433 (2018) 329–335.
[70] A. Alonso-Tellez, D. Robert, V. Keller, N. Keller, Environ. Sci. Pollut. Res. 21 (2014) 3503–3514.
[71] Á. Patzkó, R. Kun, V. Hornok, I. Dékány, T. Engelhardt, N. Schall, Colloids Surf., A 265 (2005) 64–72.
[72] J.S. Valente, F. Tzompantzi, J. Prince, J.G.H. Cortez, R. Gomez, Appl. Catal. B-Environ. 90 (2009) 330–338.
[73] W. Lv, L. Yang, B. Fan, Y. Zhao, Y. Chen, N. Lu, R. Li, Chem. Eng. J. 263 (2015) 309–316.
[74] Q. Wang, D. O'Hare, Chem. Rev. 112 (2012) 4124–4155.
[75] B.M. Choudary, S. Madhi, N.S. Chowdari, M.L. Kantam, B. Sreedhar, J. Am. Chem. Soc. 124 (2002) 14127–14136.
[76] Y. Liu, S. Chen, K. Li, J. Wang, P. Chen, H. Wang, J. Li, F. Dong, J. Colloid Interface Sci. 606 (2022) 1435–1444.
[77] J. Zou, Z. Wang, W. Guo, B. Guo, Y. Yu, L. Wu, Appl. Catal. B-Environ. 260 (2020) 118185.
[78] X. Lv, J. Zhang, X. Dong, J. Pan, W. Zhang, W. Wang, G. Jiang, F. Dong, Appl. Catal. B-Environ. 277 (2020) 119200.
[79] X.A. Dong, Z. Cui, Y. Sun, F. Dong, ACS Catal. 11 (2021) 8132–8139.
[80] C. Yang, G. Miao, Y. Pi, Q. Xia, J. Wu, Z. Li, J. Xiao, Chem. Eng. J. 370 (2019) 1128–1153.
[81] Y. Meng, T. Dai, X. Zhou, G. Pan, S. Xia, Catal. Sci. Technol. 10 (2020) 424–439.
[82] B. Shao, Z. Liu, G. Zeng, Y. Liu, Q. Liang, Q. He, T. Wu, Y. Pan, J. Huang, Z. Peng, S. Luo, C. Liang, X. Liu, S. Tong, J. Liang, Appl. Catal. B-Environ. 286 (2021) 119867.
[83] P. Chen, L. Chen, X.A. Dong, H. Wang, J. Li, Y. Zhou, C. Xue, Y. Zhang, F. Dong, ACS ES&T Eng. 1 (2021) 501–511.
[84] X. Zhang, L. Wang, X. Zhou, Z. Ni, S. Xia, ACS Sustain. Chem. Eng. 6 (2018) 13395–13407.
[85] S. Fu, Y. Zheng, X. Zhou, Z. Ni, S. Xia, J. Hazard. Mater. 363 (2019) 41–54.
[86] J. Zhang, B. Shen, Z. Hu, M. Zhen, S.-Q. Guo, F. Dong, Appl. Catal. B-Environ. 296 (2021) 120376.
[87] D. Wang, Y. Li, Adv. Mater. 23 (2011) 1044–1060.
[88] F. Wang, C. Li, L.-D. Sun, C.-H. Xu, J. Wang, J.C. Yu, C.-H. Yan, Angew. Chem. Int. Ed. 51 (2012) 4872–4876.
[89] R.J. White, R. Luque, V.L. Budarin, J.H. Clark, D.J. Macquarrie, Chem. Soc. Rev. 38 (2009) 481–494.
[90] Z. Yang, W.W. Tjiu, W. Fan, T. Liu, Electrochim. Acta 90 (2013) 400–407.
[91] F. Zhang, X. Zhao, C. Feng, B. Li, T. Chen, W. Lu, X. Lei, S. Xu, ACS Catal. 1 (2011) 232–237.
[92] L. Li, L. Dou, H. Zhang, Nanoscale 6 (2014) 3753–3763.
[93] J.H. Lee, H. Kim, Y.S. Lee, D.-Y. Jung, ChemCatChem 6 (2014) 113–118.
[94] X. Zou, A. Goswami, T. Asefa, J. Am. Chem. Soc. 135 (2013) 17242–17245.
[95] S. Kumar, M.A. Isaacs, R. Trofimovaite, L. Durndell, C.M.A. Parlett, R.E. Douthwaite, B. Coulson, M.C.R. Cockett, K. Wilson, A.F. Lee, Appl. Catal. B-Environ. 209 (2017) 394–404.
[96] X. Yuan, W. Li, Appl. Clay Sci. 138 (2017) 107–113.
[97] K.-I. Katsumata, K. Sakai, K. Ikeda, G. Carja, N. Matsushita, K. Okada, Mater. Lett. 107 (2013) 138–140.
[98] Z. Li, Q. Zhang, X. Liu, L. Wu, H. Hu, Y. Zhao, J. Mater. Sci. 53 (2018) 12795–12806.
[99] Z. Li, M. Chen, H. Hu, Q. Zhang, D. Tao, J. Solid State Chem. 290 (2020) 121594.
[100] Y. Tian, T. Tatsuma, J. Am. Chem. Soc. 127 (2005) 7632–7637.
[101] J. Van Durme, J. Dewulf, W. Sysmans, C. Leys, H. Van Langenhove, Chemosphere 68 (2007) 1821–1829.
[102] X. Jin, K. Taniguchi, K. Yamaguchi, N. Mizuno, Chem. Sci. 7 (2016) 5371–5383.
[103] J.S. Valente, F. Tzompantzi, J. Prince, Appl. Catal. B-Environ. 102 (2011) 276–285.
[104] H. Li, J. Li, C. Xu, P. Yang, D.H.L. Ng, P. Song, M. Zuo, J. Alloys Compd. 698 (2017) 852–862.
[105] L. Wang, X. Gao, Y. Cheng, X. Zhang, G. Wang, Q. Zhang, J. Su, J. Photochem, Photobiol., A 369 (2019) 44–53.
[106] S. Nayak, L. Mohapatra, K. Parida, J. Mater. Chem. A 3 (2015) 18622–18635.
[107] W. Zhang, Z. Wang, Y. Zhao, H.N. Miras, Y.-F. Song, ChemCatChem 11 (2019) 5466–5474.
[108] M. Fang, G.F. Dong, R.J. Wei, J.C. Ho, Adv. Energy Mater. 7 (2017) 25.
[109] W. Xi, G. Yan, H. Tan, L. Xiao, S. Cheng, S.U. Khan, Y. Wang, Y. Li, Dalton Trans. 47 (2018) 8787–8793.
[110] Z. Yang, Y. Zhang, C. Feng, H. Wu, Y. Ding, H. Mei, Int. J. Hydrogen Energy 46 (2021) 25321–25331.
[111] R. Guo, H. Wen, S. Zhang, T. Yu, Y. He, Z. Ni, J. You, Mater. Lett. 285 (2021) 129132.
[112] E.M. Seftel, M. Niarchos, N. Vordos, J.W. Nolan, M. Mertens, A.C. Mitropoulos, E.F. Vansant, P. Cool, Micropor. Mesopor. Mater. 203 (2015) 208–215.
[113] G. Mendoza-Damián, F. Tzompantzi, A. Mantilla, R. Pérez-Hernández, A. Hernández-Gordillo, Appl. Clay Sci. 121–122 (2016) 127–136.
[114] S. Li, C.I. Ezugwu, S. Zhang, Y. Xiong, S. Liu, Appl. Surf. Sci. 487 (2019) 260–271.
[115] C. Wang, B. Ma, S. Xu, D. Li, S. He, Y. Zhao, J. Han, M. Wei, D.G. Evans, X. Duan, Nano Energy 32 (2017) 463–469.
[116] S. Xia, Y. Meng, X. Zhou, J. Xue, G. Pan, Z. Ni, Appl. Catal. B-Environ. 187 (2016) 122–133.
[117] S. Xia, G. Zhang, Y. Meng, C. Yang, Z. Ni, J. Hu, Appl. Catal. B-Environ. 278 (2020) 119266.
[118] C. Yang, G. Zhang, Y. Meng, G. Pan, Z. Ni, S. Xia, J. Hazard. Mater. 408 (2021) 124908.
[119] L. Zhang, Y. Meng, H. Shen, J. Li, C. Yang, B. Xie, S. Xia, Appl. Surf. Sci. 567 (2021) 150760.
[120] L. Wang, X. Gao, J. Su, Q. Zhang, K. Zheng, Z. Zhang, J. Photochem, Photobiol., A, 383 (2019) 111973.
[121] Y. Lyu, C. Li, X. Du, Y. Zhu, Y. Zhang, S. Li, Fuel 262 (2020) 116610.
[122] Y. Zhang, C. Li, Y. Zhu, X. Du, Y. Lyu, S. Li, Y. Zhai, Fuel 276 (2020) 118099.
[123] Z. Abbasi, M. Haghighi, E. Fatehifar, S. Saedy, J. Hazard. Mater. 186 (2011) 1445–1454.
[124] T. Baskaran, J. Christopher, A. Sakthivel, RSC Adv. 5 (2015) 98853–98875.
[125] S. Huang, B. Cheng, J. Yu, C. Jiang, A.C.S. Sustain, Chem. Eng. 6 (2018) 12481–12488.
[126] Z. Yan, Z. Xu, J. Yu, M. Jaroniec, J. Colloid Interface Sci. 501 (2017) 164–174.
[127] B.-B. Chen, X.-B. Zhu, M. Crocker, Y. Wang, C. Shi, Catal. Commun. 42 (2013) 93–97.
[128] J. Ye, B. Cheng, S. Wageh, A.A. Al-Ghamdi, J. Yu, RSC Adv. 6 (2016) 34280–34287.
[129] Z. Yan, Z. Xu, L. Yue, L. Shi, L. Huang, Chin. J. Catal. 39 (2018) 1919–1928.
[130] Y. Xu, Z. Wang, L. Tan, H. Yan, Y. Zhao, H. Duan, Y.-F. Song, Ind. Eng. Chem. Res. 57 (2018) 5259–5267.
[131] Y. Xu, Z. Wang, L. Tan, Y. Zhao, H. Duan, Y.-F. Song, Ind. Eng. Chem. Res. 57 (2018) 10411–10420.
[132] Z. Ni, Q. Wang, P. Yao, X. Liu, Y. Li, Acta Chim. Sinica 69 (2011) 529–535.
[133] H.M.S. Al-Aani, E. Iro, P. Chirra, I. Fechete, M. Badea, C. Negrilă, I. Popescu, M. Olea, I.-C. Marcu, Appl. Catal. A-Gen. 586 (2019) 117215.
[134] A.F. Al-Hossainy, A. Ibrahim, M.S. Zoromba, J. Mater. Sci-Mater. Electron 30 (2019) 11627–11642.
[135] K. Yan, Y. Liu, Y. Lu, J. Chai, L. Sun, Catal. Sci. Technol. 7 (2017) 1622–1645.
[136] S.-T. Zhang, Y. Dou, J. Zhou, M. Pu, H. Yan, M. Wei, D.G. Evans, X. Duan, ChemPhysChem 17 (2016) 2754–2766.
[137] Z. Li, H. Duan, M. Shao, J. Li, D. O'Hare, M. Wei, Z.L. Wang, Chem 4 (2018) 2168–2179.
[138] G. Cui, X. Meng, X. Zhang, W. Wang, S. Xu, Y. Ye, K. Tang, W. Wang, J. Zhu, M. Wei, D.G. Evans, X. Duan, Appl. Catal. B-Environ. 248 (2019) 394–404.
[139] K. Jirátová, F. Kovanda, J. Ludvíková, J. Balabánová, J. Klempa, Catal. Today 277 (2016) 61–67.
[140] Z. Lv, Q. Chen, Y. Guo, Solid State Sci. 109 (2020) 106393.
[141] L. Nie, G. Fan, A. Wang, L. Zhang, J. Guan, N. Han, Y. Chen, Sens. Actuat. B-Chem. 345 (2021) 130412.
[142] Z. Li, Q. Yan, Q. Jiang, Y. Gao, T. Xue, R. Li, Y. Liu, Q. Wang, Appl. Catal. B-Environ. 269 (2020) 118827.
[143] J. Deng, S. He, S. Xie, H. Yang, Y. Liu, G. Guo, H. Dai, Environ. Sci. Technol. 49 (2015) 11089–11095.
[144] M.H. Castaño, R. Molina, S. Moreno, Appl. Catal. A-Gen. 492 (2015) 48–59.
[145] Y. Zhang, Y. Lin, Z. Huang, G. Jing, H. Zhao, X. Wu, S. Zhang, Energy Fuels. 35 (2021) 743–751.
[146] W. Deng, B. Gao, Z. Jia, D. Liu, L. Guo, Catal. Sci. Technol. 11 (2021) 5094–5108.
[147] Q. Zhao, Q. Liu, C. Song, N. Ji, D. Ma, X. Lu, Chemosphere 218 (2019) 895–906.
[148] Y. Sun, X. Zhang, N. Li, X. Xing, H. Yang, F. Zhang, J. Cheng, Z. Zhang, Z. Hao, Appl. Catal. B-Environ. 251 (2019) 295–304.
[149] Q. Yang, D. Wang, C. Wang, K. Li, Y. Peng, J. Li, ChemCatChem 10 (2018) 4838–4843.
[150] D. Wang, Q. Yang, G. Yang, S. Xiong, X. Li, Y. Peng, J. Li, J. Crittenden, Chem. Eng. J. 399 (2020) 125792.
[151] T. Xue, R. Li, Y. Gao, Q. Wang, Chem. Eng. J. 384 (2020) 123284.
[152] T. Xue, R. Li, Z. Zhang, Y. Gao, Q. Wang, J. Environ. Sci. 96 (2020) 194–203.
[153] D.M. Gómez, J.M. Gatica, J.C. Hernández-Garrido, G.A. Cifredo, M. Montes, O. Sanz, J.M. Rebled, H. Vidal, Appl. Catal. B-Environ. 144 (2014) 425–434.
[154] S. Mo, S. Li, J. Li, Y. Deng, S. Peng, J. Chen, Y. Chen, Nanoscale 8 (2016) 15763–15773.
[155] Q. Zhao, Y. Ge, K. Fu, N. Ji, C. Song, Q. Liu, Chemosphere 204 (2018) 257–266.
[156] S. Li, H. Wang, W. Li, X. Wu, W. Tang, Y. Chen, Appl. Catal. B-Environ. 166–167 (2015) 260–269.
[157] S. Li, S. Mo, J. Li, H. Liu, Y. Chen, RSC Adv. 6 (2016) 56874–56884.
[158] D. Li, Y. Fan, Y. Ding, X. Wei, Y. Xiao, Catal. Commun. 88 (2017) 60–63.
[159] S. Mo, S. Li, J. Li, S. Peng, J. Chen, Y. Chen, Catal. Commun. 87 (2016) 102–105.
[160] S. Mo, S. Li, W. Li, J. Li, J. Chen, Y. Chen, J. Mater. Chem. A 4 (2016) 8113–8122.
[161] W. Li, S. Yang, K. Wang, S. Tu, M. Lu, P. Wu, React. Kinet. Mech. Cat. 128 (2019) 965–977.
[162] Y.-G. Yan, Z.-J. Mao, J.-J. Luo, R.-P. Du, J.-X. Lin, J. Fuel Chem. Technol. 48 (2020) 1452–1460.
[163] M. Dios, J.A. Souto, J.J. Casares, Energy 53 (2013) 40–51.
[164] S.-J. Chen, J.-K. Hsu, W.-J. Lee, J.-T. Lee, C.-J. Su, J. Aerosol Sci 28 (1997), S261–S262.
[165] Z. Li, Y. Wang, Y. Hu, L. Chen, H. Zhu, Aerosol Air Qual. Res. 19 (2019) 2056–2069.
[166] M. Ahmed, B. Rappenglück, S. Das, S. Chellam, Environ. Adv. 6 (2021) 100127.
[167] C.H. Ao, S.C. Lee, J.Z. Yu, J.H. Xu, Appl. Catal. B-Environ. 54 (2004) 41–50.
[168] X. Ma, L. Yang, H. Wu, J. Clean. Prod. 302 (2021) 126925.
[169] X. Cao, J. Lu, X. Zheng, D. He, W. Zhu, Y. Zhao, W. Zhang, R. Tian, Y. Luo, Chem. Eng. J. 429 (2022) 132473.
[170] Z. Ma, L. Sheng, X. Wang, W. Yuan, S. Chen, W. Xue, G. Han, Z. Zhang, H. Yang, Y. Lu, Y. Wang, Adv. Mater. 31 (2019) 1903719.

[171] Y. Zhu, C. Li, Y. Lyu, S. Li, Y. Zhang, X. Du, Y. Zhai, J. Hazard. Mater. 402 (2021) 123502.
[172] R.K. Kaila, A. Gutiérrez, A.O.I. Krause, Appl. Catal. B-Environ. 84 (2008) 324–331.
[173] B. Hua, N. Yan, M. Li, Y.-F. Sun, J. Chen, Y.-Q. Zhang, J. Li, T. Etsell, P. Sarkar, J.-L. Luo, J. Mater. Chem. A 4 (2016) 9080–9087.
[174] Y. Ma, X. Wang, P. Ning, C. Cheng, K. Xu, F. Wang, Z. Bian, S. Yan, Chem. Eng. J. 290 (2016) 328–334.
[175] H. Wang, H. Yi, X. Tang, P. Ning, L. Yu, D. He, S. Zhao, K. Li, Appl. Clay Sci. 70 (2012) 8–13.
[176] R. Sui, C.B. Lavery, C.E. Deering, R. Prinsloo, D. Li, N. Chou, K.L. Lesage, R.A. Marriott, Appl. Catal. A-Gen. 604 (2020) 117773.
[177] E. Kamp, H. Thielert, O. von Morstein, S. Kureti, N. Schreiter, J.-U. Repke, Catal, Sci. Technol. 10 (2020) 2961–2969.
[178] M.A. Othman, W.M. Zahid, A.E. Abasaeed, J. Hazard. Mater. 254–255 (2013) 221–227.
[179] D.E. Sparks, T. Morgan, P.M. Patterson, S.A. Tackett, E. Morris, M. Crocker, Appl. Catal. B-Environ. 82 (2008) 190–198.
[180] Q. Hong, H. Xu, Y. Yuan, Y. Shen, Y. Wang, W. Huang, Z. Qu, N. Yan, Chem. Eng. J. 400 (2020) 125963.
[181] Y. Yuan, H. Xu, W. Liu, L. Chen, Z. Quan, P. Liu, Z. Qu, N. Yan, J. Colloid Interface Sci. 536 (2019) 431–439.
[182] S. Zhao, H. Yi, X. Tang, C. Song, Chem. Eng. J. 226 (2013) 161–165.
[183] Y. Nie, Q. Yan, S. Chen, D. O'Hare, Q. Wang, Catal. Commun. 97 (2017) 47–50.
[184] X. Wu, Y. Feng, X. Liu, L. Liu, Y. Du, Z. Li, Appl. Surf. Sci. 495 (2019) 143513.
[185] Q. Yan, S. Chen, C. Zhang, Q. Wang, B. Louis, Appl. Catal. B-Environ. 238 (2018) 236–247.
[186] S. Jayaprakash, N. Dewangan, A. Jangam, S. Kawi, Fuel Process. Technol. 219 (2021) 106871.
[187] H. Huang, Y. Xu, Q. Feng, D.Y.C. Leung, Catal, Sci. Technol. 5 (2015) 2649–2669.
[188] Z. Wang, S. Li, S. Xie, Y. Liu, H. Dai, G. Guo, J. Deng, Appl. Catal. A-Gen. 579 (2019) 106–115.
[189] Y. Liu, H. Dai, J. Deng, S. Xie, H. Yang, W. Tan, W. Han, Y. Jiang, G. Guo, J. Catal. 309 (2014) 408–418.
[190] H. Sheng, Q. Li, W. Ma, H. Ji, C. Chen, J. Zhao, Appl. Catal. B-Environ. 138–139 (2013) 212–218.
[191] Z. Liu, R. Ma, M. Osada, N. Iyi, Y. Ebina, K. Takada, T. Sasaki, J. Am. Chem. Soc. 128 (2006) 4872–4880.
[192] B.M. Hunter, H.B. Gray, A.M. Müller, Chem. Rev. 116 (2016) 14120–14136.
[193] P. Salvador, J. Phys. Chem. C 111 (2007) 17038–17043.
[194] D.W. Kwon, P.W. Seo, G.J. Kim, S.C. Hong, Appl. Catal. B-Environ. 163 (2015) 436–443.
[195] F. Rodriguez-Rivas, A. Pastor, C. Barriga, M. Cruz-Yusta, L. Sánchez, I. Pavlovic, Chem. Eng. J. 346 (2018) 151–158.
[196] Q. Yan, X. Hou, G. Liu, Y. Li, T. Zhu, Y. Xin, Q. Wang, J. Hazard. Mater. 400 (2020) 123260.
[197] R. Mrad, R. Cousin, N.A. Saliba, L. Tidahy, S. Siffert, C. R. Chim. 18 (2015) 351–357.
[198] D. Yuan, X. Li, Q. Zhao, J. Zhao, M. Tadé, S. Liu, J. Catal. 309 (2014) 268–279.
[199] E. Genty, H. Dib, J. Brunet, C. Poupin, S. Siffert, R. Cousin, Top. Catal. 62 (2019).
[200] E. Genty, C. Serhal, R. El Khawaja, H. Dib, M. Labaki, I. Mallard, C. Poupin, S. Siffert, R. Cousin, J. Nanosci. Nanotechnol. 20 (2020) 1130–1139.
[201] R. Li, T. Xue, R. Bingre, Y. Gao, B. Louis, Q. Wang, A.C.S. Appl, Mater. Inter. 10 (2018) 34834–34839.
[202] P.Q. Cui, H.G. Zhou, C. Li, S.P. Wu, Y. Xiao, Constr. Build. Mater. 123 (2016) 69–77.
[203] P. Cui, S. Wu, Y. Xiao, M. Wan, P. Cui, J. Clean. Prod. 108 (2015) 987–991.
[204] L. Vigna, A. Nigro, A. Verna, I.V. Ferrari, S.L. Marasso, S. Bocchini, M. Fontana, A. Chiodoni, C.F. Pirri, M. Cocuzza, ACS Omega 6 (2021) 20205–20217.
[205] N. Han, P. Hu, A. Zuo, D. Zhang, Y. Tian, Y. Chen, Sens. Actuat. B-Chem. 145 (2010) 114–119.
[206] C. Doornkamp, V. Ponec, J. Mol. Catal. A: Chem. 162 (2000) 19–32.
[207] G. Guan, M. Kaewpanha, X. Hao, A. Abudula, Renew. Sust. Energ. Rev. 58 (2016) 450–461.
[208] G. Mitran, D.G. Mieritz, D.-K. Seo, J. Saudi Chem. Soc. 23 (2019) 916–924.
[209] G. Mitran, D.G. Mieritz, D.-K. Seo, Int. J. Hydrogen Energy 42 (2017) 21732–21740.
[210] S. Tang, Y. Yao, T. Chen, D. Kong, W. Shen, H.K. Lee, Anal. Chim. Acta 1103 (2020) 32–48.
[211] S. Jin, P.H. Fallgren, J.M. Morris, Q. Chen, Sci. Technol. Adv. Mater. 8 (2007) 67–70.
[212] J. Wang, G. Lv, C. Wang, Appl. Surf. Sci. 570 (2021) 151182.
[213] Y. Yang, Y. Xie, Z. Yu, S. Guo, M. Yuan, H. Yao, Z. Liang, Y.R. Lu, T.-S. Chan, C. Li, H. Dong, S. Ma, Chem. Eng. J. 419 (2021) 129512.
[214] M. Flores-Flores, E. Luévano-Hipólito, L.M.T. Martínez, G. Morales-Mendoza, R. Gómez, J. Photochem, Photobiol., A 363 (2018) 68–73.
[215] N. Dewangan, W.M. Hui, S. Jayaprakash, A.-R. Bawah, A.J. Poerjoto, T. Jie, A. Jangam, K. Hidajat, S. Kawi, Catal. Today 356 (2020) 490–513.
[216] B. Zhu, Q. Xu, X. Bao, H. Yin, Y. Qin, X.-C. Shen, Chem. Eng. J. 429 (2022) 132284.
[217] S. Xia, L. Fang, Y. Meng, X. Zhang, L. Zhang, C. Yang, Z. Ni, Appl. Catal. B-Environ. 272 (2020) 118949.
[218] M. Zhang, L. Mei, L. Zhang, X. Wang, X. Liao, X. Qiao, C. Hong, Bioelectrochemistry 142 (2021) 107943.
[219] L. Ju, P. Wu, X. Lai, S. Yang, B. Gong, M. Chen, N. Zhu, Environ. Pollut. 228 (2017) 234–244.
[220] M. Pavel, G. Layrac, F. Papa, C. Negrilă, D. Tichit, I.-C. Marcu, Catal. Today 306 (2017).